6-2000

Stereoselection in the preparation of alpha-OXY-beta-amino esters : revealing the mechanism

Richard James Fox
Union College - Schenectady, NY

STEREOSELECTION IN THE PREPARATION OF α-OXY-β-AMINO ESTERS: REVEALING THE MECHANISM

By

Richard James Fox

****

Submitted in partial fulfillment

of the requirements for

Honors in the Department of Chemistry

UNION COLLEGE

June, 2000

ABSTRACT

FOX, RICHARD J Stereoselection in the Preparation of α-Oxy-β-Amino Esters: Revealing the Mechanism. Department of Chemistry, June 2000.

Due to their significant pharmaceutical applications, the development of efficient, stereoselective synthetic routes for the preparation of α-substituted-β-amino esters has become increasingly important. We demonstrated that the titanium enolates (**47**) of α-alkoxy acetate esters (**48**) add cleanly to imines (**49**), and predominately afford the *anti* diastereomer of the α-oxy-β-amino ester product (**50**). Furthermore, by altering the electronic properties of the ether oxygen, sterics of the ester and temperature conditions, we changed the *anti*:*syn* product ratio. We rationalized the origin of these effects, and proposed a mechanism of imine addition.

Acknowledgements

To the most unselfish Dr. Patricia Fox, without whose generosity I may have never had the wonderful opportunity to attend Union College.

To my parents and family members who taught me to value my education, and always allowed me to pursue my goals.

To Kathleen for putting up with my long hours in the lab, and smell of organic solvents.

Finally, to Professor James C. Adrian Jr. for providing me with more knowledge than I can retain at this time, and the perfect balance between assistance and freedom that a mentor should supply.

Table of Contents

Table of Figures

Introduction

Due to their significant pharmaceutical applications, the development of efficient, stereoselective synthetic routes for the preparation of α-substituted-β-amino esters has become increasingly important. Taxol (**1**) is one such example that clearly demonstrates the importance of this research area.[1]

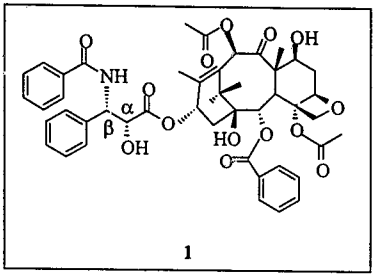

1

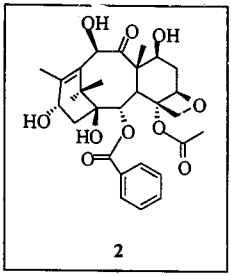

2

Taxol is an important molecule since it possesses strong anti-tumor activity towards previously untreatable forms of cancer. Unfortunately, the world supply of Taxol depends entirely on its extraction from the bark of the slow growing Pacific yew tree (*Taxus brevifolia*).[1] Numerous groups have recognized this problem, and developed total syntheses of Taxol.[2,3] In addition, it has been shown that the 10-deacetylbaccatin III moiety of Taxol (**2**) is readily available from the leaves of the European yew (*Taxus baccata*).[1] Consequently, numerous groups have focused solely on the stereoselective preparation of the *syn* (2R, 3S), α-oxy-β-amino ester, side chain of **1**.[1,4]

Adding to the importance of α-substituted-β-amino esters is their role as intermediate species (**3**) in the syntheses of β-lactams (**4**), many of which like the penicillin family of antibiotics have important pharmaceutical applications (Scheme 1).[5]

Scheme 1

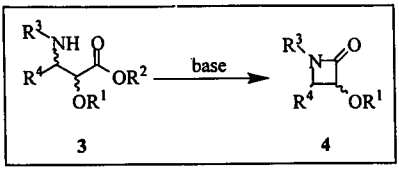

3 4

Numerous groups have stereoselectively prepared α,β-disubstituted carbonyl containing compounds using aldol and imine-aldol additions based on the general procedure developed by Evans and coworkers.[6] For example, Vilarrasa and coworkers examined the aldol addition between the chloro titanium enolates of chiral α-O-protected ketones (**5**) and various aldehydes (**6**) (Scheme 2).[7]

Scheme 2

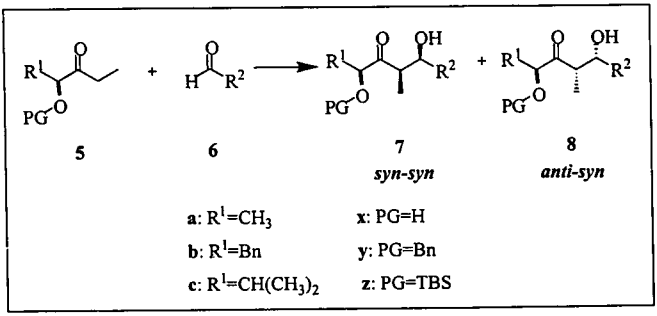

5 6 7 *syn-syn* 8 *anti-syn*

a: R^1=CH_3 **x**: PG=H

b: R^1=Bn **y**: PG=Bn

c: R^1=$CH(CH_3)_2$ **z**: PG=TBS

It was shown that the type **5x** ketones proceeded with poor yields and diastereoselectivities. In addition, despite the improved yields for the type **5y** ketones, only moderate *syn-syn* selectivity was observed: 5:1 (**7**:**8**) from **5ay**, R^2 = *i*-Pr, 4:1 from

5by, R^2 = *i*-Pr, 1:1 from **5cy**, R^2 = *i*-Pr.[7] On the other hand, the type **5z** ketones proceeded with high yields and excellent *syn-syn* selectivity: 30:1 (**7**:**8**) from **5az**, R^2 = *i*-Pr, 35:1 from **5bz**, R^2 = *i*-Pr, >95:1 from **5cz**, R^2 = *i*-Pr.[7] Finally, the researchers observed that the nature of R^2 affected some of the ratios for the type **5z** ketones: 30:1 (**7**:**8**) from **5az**, R^2 = Pr, 45:1 from **5bz**, R^2 = [$C(CH_3)=CH_2$], 50:1 from **5cz**, R^2 = Ph.[7] The researchers proposed that the improved *syn-syn* diastereoselectivities for the **5z**, as opposed to **5y**, ketones suggested different transition states.

Due to the increased lewis basicity of the type **5y** ketones, the researchers proposed that a chelated titanium enolate (**9**) predominated at equilibrium, and transition states **10** and **11** would lead to either diastereomer (Scheme 3).[7]

Scheme 3

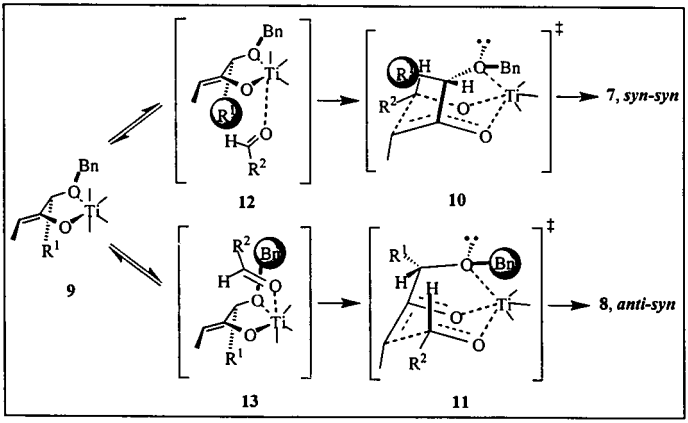

Scheme 3 showed how the aldehydes approach to **9** could influence diastereomer formation. For example, the *syn-syn* product (**7**) formed when the aldehyde approached **9**

from below as in **12**, while the *anti-syn* product (**8**) formed when the aldehyde approached **9** from above as in **13**. The high steric hindrance between R^1 and R^2 in **12**, and R^2 and Bn in **13** supported the poor diastereoselectivities observed for the type **5y** ketones.

On the contrary, due to the decreased lewis basicity of the type **5z** ketones, it was proposed that an unchelated titanium enolate (**14**) predominated at equilibrium, and transition states **15** and **16** would lead to either diastereomer (Scheme 4).[7]

Scheme 4

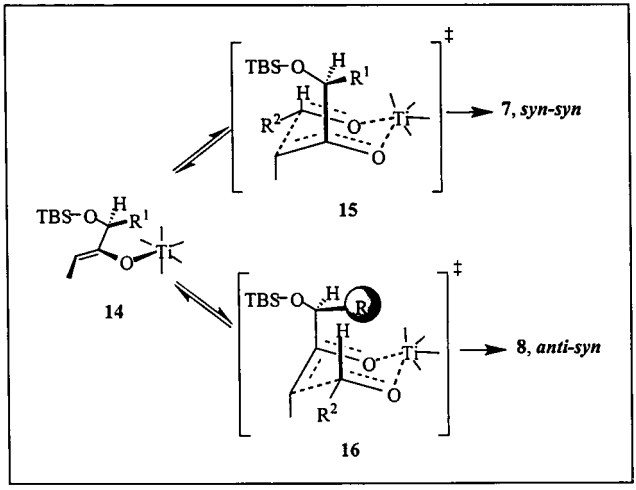

It was revealed that higher *syn-syn* selectivities were observed for the type **5z** ketones as the size of R^1 and R^2 increased due to the steric destabilization of **16**. In addition to the high *syn* discrimination shown by Vilarrasa, other groups have observed both *syn* and *anti* selectivity.

Cozzi and coworkers performed aldol condensations between the chloro titanium enolates of α-alkoxy thio esters (**17**) and various aldehydes (**18**) (Scheme 5).[8]

Scheme 5

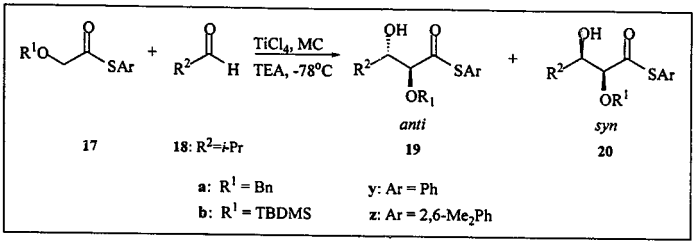

It was found that regardless of the size of R^2, when R^1 = benzyl (**17a**), the *anti* diastereomer predominated, 98:2 (**19ay**:**20ay**), while the *syn* diastereomer predominated when R^1 = TBDMS (**17b**), 10:90 (**19by**:**20by**).[8] In addition, it was shown that the *anti* selectivity decreased when the size of Ar increased (**17az**), 63:67 (**19az**:**20az**). Cozzi and coworkers proposed that two different enolates proceeding through similar transition states could explain the opposing stereoselectivity.[8]

In agreement with Vilarrasa[7], Cozzi and coworkers proposed that the differing lewis basicities of thio esters **17a** and **17b** controlled diastereomer formation. For example, due to the increased lewis basicity of the type **17a** thio esters, the researchers proposed that a chelated (E)-titanium enolate predominated at equilibrium. On the other hand, as a result of the larger and less lewis basic TBDMS group, they proposed that an unchelated (Z)-titanium enolate predominated at equilibrium for thio esters of the type **17b**. Based on this hypothesis, which was supported by ^{1}H-NMR, Cozzi and coworkers proposed the following transition states (Figure 1).[8]

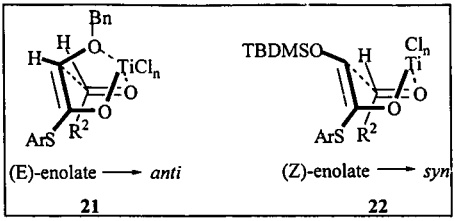

Figure 1. Cozzi transition states

From Figure 1, it is clear that Cozzi proposed the chelated (E)-enolate could have proceeded through a bicyclic boat transition state (**21**) to afford the *anti* product (**19**), while the unchelated (Z)-enolate could have formed an open boat transition state (**22**) to yield the *syn* isomer (**20**). In addition to Cozzi, Hanoaka and coworkers also observed stereoselection for both of their diastereomeric products.

Hanaoka and coworkers investigated aldol condensations between chiral chromium-complexed aldehydes (**23**), and the various metal enolates of α-alkoxy oxy and thio esters (**24**) (Scheme 6).[9]

Scheme 6

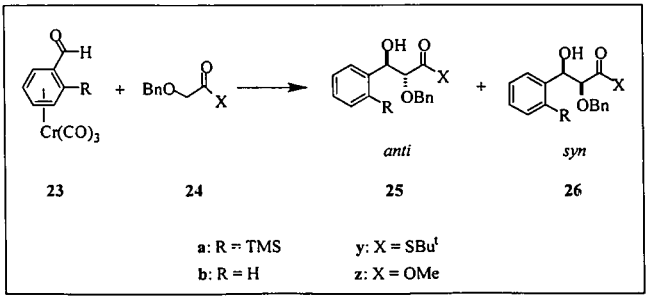

These researchers showed that the diastereoselectivity depended on the nature of the metal enolate. For example, the addition of **23a** to the lithium and titanium enolate of **24y** proceeded with *syn* (20:80, **25ay**:**26ay**), and *anti* (95:5, **25ay**:**26ay**) selectivity respectively.[9] Furthermore, it was also shown that the diastereomeric ratio for the condensation between **23a** and the chloro titanium enolate of **24z** dropped to 38:62 (**25az**:**26az**).[9] Finally, since the diastereomeric ratio for the condensation between **23b** and the chloro titanium enolate of **24y** equaled 92:8 (**25by**:**26by**), they concluded that the R group of **23** did not alter the *anti* selectivity.[9] Despite their uncertainty in the nature of the chloro-titanium enolates, the researchers proposed that the observed *anti* selectivity could have arisen from a chelated (E)-enolate, and cyclic boat-like transition state analogous to **21**.[9] Conversely, they proposed that the lithium enolate of **24y** could have adopted an (E)- or (Z)- configuration, and proceeded through a cyclic chair-like transition state to afford either the *syn* or *anti* diastereomer respectively.[9]

Contrary to the previous examples, Ghosh and coworkers required *two* equivalents of lewis acid for the aldol condensations between the chloro titanium enolates of *p*-toluenesulfonamido esters (**27**) and various aldehydes (**28**) to occur (Scheme 7).[10]

Scheme 7

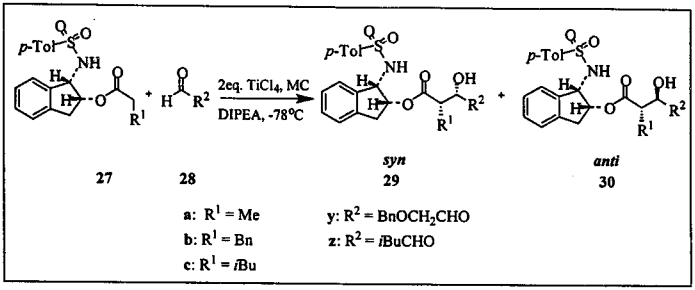

In addition, they found that oxyaldehydes of the type **28y** proceeded with excellent *syn* selectivity (98:2, **29ay**:**30ay**), while aliphatic aldehydes of the type **28z** afforded exceptional *anti* selectivity (1:99, **29az**:**30az**).[10] Furthermore, it was observed that the size or electronics of R^1 did not affect the diastereomeric product ratio: 99:1, **29by**:**30by**, 99:1, **29cy**:**30cy**.[10] In previous work, Ghosh and coworkers proposed a Zimmerman-Traxler chair-like transition state (**31**) to rationalize the *anti* selectivity (Figure 2).[11] Based on this model, the researchers postulated that the *syn* selectivity resulted from the addition of the chelating oxygen substituent on aldehydes of the type **28y**, which could have proceeded through transition state **32** (Figure 2).[10]

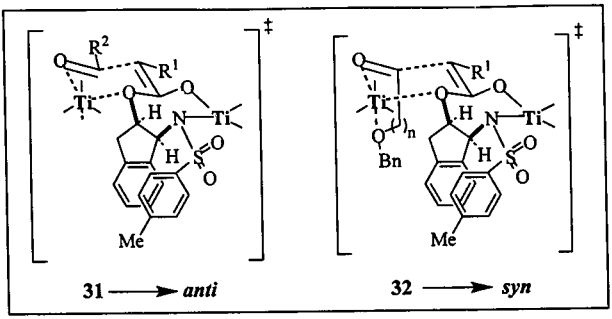

Figure 2. Ghosh transition states

Figure 2 showed that like Vilarrasa[7] and Cozzi[8], the observed selectivity depended on the ability of the lewis basic oxyaldehyde substituent to chelate with one of the titanium metals. In addition to the numerous aldol condensations mentioned above, other groups have also studied stereoselective imine-aldol additions.

Due to their inherent chirality and function as an easily removed amine protecting group, Ellman and coworkers investigated the imine-aldol condensations between *tert*-butanesulfinyl imines (**33**), and the isopropoxide titanium-ate enolate complex of methyl propionate (**34**) (Scheme 8).[12]

Scheme 8

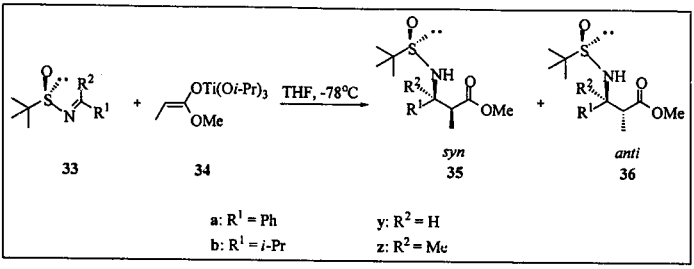

These researchers found that regardless of R^1 and R^2, the addition afforded exceptional *syn* selectivity: 98:2, **35ay**:**36ay**, 98:2, **35az**:**36az**, 98:2, **35by**:**36by**, 99:1, **35bz**:**36bz**. In order to rationalize this selectivity, the researchers proposed that the enolate adopted an (E)-conformation, and proceeded through a Zimmerman-Traxler chair-like transition state (**37**) (Figure 3).[12]

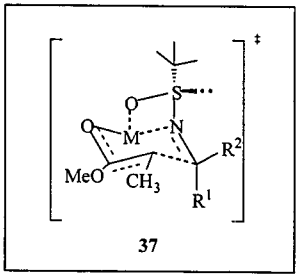

Figure 3. Ellman chair transition state

The present research in our laboratory focuses on the preparation of α-oxy-β-amino esters through the imine-aldol addition of the chloro-titanium enolates of α-alkoxy

acetate esters. In previous work, Barkin investigated the effects of imine substitution on product diastereoselectivity using the chloro-titanium enolate (**38**) of methyl methoxy acetate (**39**) (Scheme 9).

Scheme 9

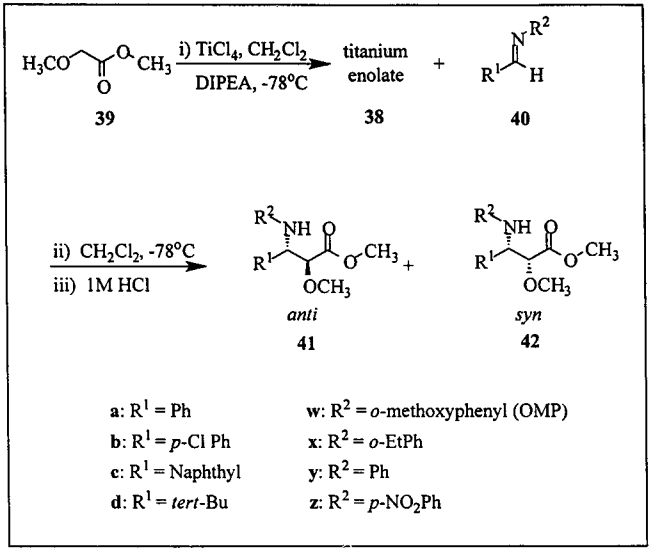

39 **38** **40**

41 **42**

It is important to note here that unlike Ghosh[10], Barkin only required *one* equivalent of lewis acid ($TiCl_4$) to achieve high yield additions. While conducting this study, the major diastereomer of imine **40bw** spontaneously crystallized whose *anti* configuration was verified by X-ray crystallography (Figure 4).[13]

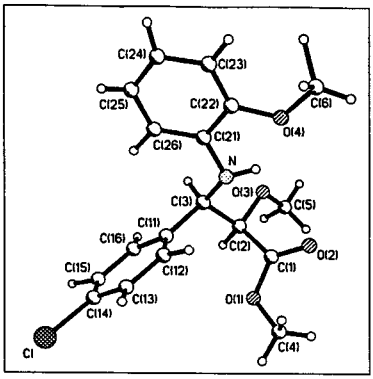

Figure 4. X-ray crystal structure of **41bw**

Serendipitously, the minor diastereomer of imine **40aw** spontaneously crystallized whose *syn* configuration was also confirmed by X-ray crystallography (Figure 5).[13]

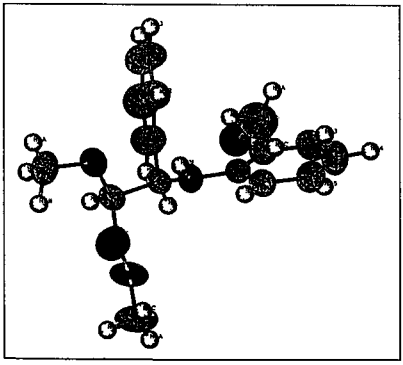

Figure 5. X-ray crystal structure of **42aw**

Based on these two results, the diastereomeric ratios for each product were easily determined by analogy using ^{1}H-NMR and crude HPLC.

Barkin found that the size of R^1 did not affect the *anti* selectivity: 94:6, **41aw**:**42aw**, 95:5, **41bw**:**42bw**, 92:8, **41cw**:**42cw**. Even though the size of R^1 did not have an affect, no addition was detected for the aliphatic imine **40dw**. Furthermore, Barkin demonstrated that the substitution of R^2 affected the degree of *anti* selectivity. For example, Barkin observed exceptional *anti* selectivities in the presence of an *ortho* substituent other than hydrogen on the phenyl ring at R^2: 94:6, **41aw**:**42aw**, 92:8, **41ax**:**42ax**. On the other hand, when the *ortho* substituent on the phenyl ring of R^2 was hydrogen, Barkin only detected moderate *anti* selectivity: 78:22, **41ay**:**42ay**, 77:23, **41az**:**42az**. Based on these data, and those collected by the researchers described earlier, a mechanism for this addition was proposed (Scheme 10).

Scheme 10

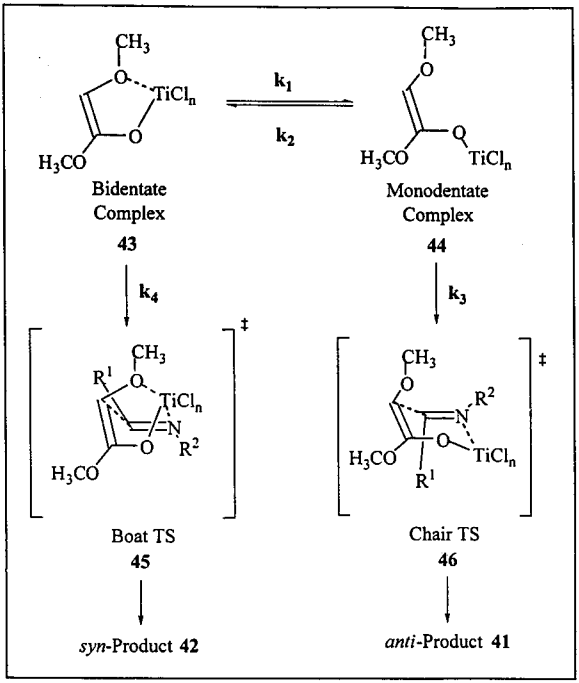

Unlike Cozzi and coworkers[8], both diastereomeric products in Scheme 10 arose from (Z)-enolates. Although, in agreement with Villarasa[7], Cozzi[8] and Ghosh[10], Scheme 10 postulated that an equilibrium existed between a bidentate chelated (**43**) and monodentate unchelated (**44**) enolate, leading to the *syn* (**42**) and *anti* (**41**) products respectively. Despite the apparent contradictions, having a chelated enolate (**43**) proceed through a bicyclic boat transition state (**45**) to afford the *syn* product (**42**), and an

unchelated enolate (**44**) leading through a Zimmerman-Traxler chair-like transition state (**46**) to afford the *anti* product, agreed with the mechanisms proposed by Cozzi[8] and Ellman[12].

Cozzi proposed that their *anti* product resulted from a bidentate (E)-enolate which proceeded through a bicyclic boat transition state (Figure 1).[8] On the other hand, Scheme 10 predicted that a bidentate (Z)-enolate proceeded through a bicylic boat transition state to afford the *syn* product. To rationalize these seeming inconsistencies, it is imperative to recall two features of Cozzi's work. First, Cozzi worked with thio esters, and since sulfur outranks oxygen due to its higher atomic number, Cozzi's (E)-enolate was structurally analogous to the (Z)-enolate in Scheme 10. But, Cozzi investigated aldol, as opposed to imine-aldol, additions. This was important since the nitrogen of an imine, unlike the oxygen of an aldehyde, is substituted; restricting the allowable conformations an imine may adopt in a given transition state. By comparing the conformations of the aldehyde and imine in transition states **21** and **45** respectively, it was clear why the bicyclic boat transition state in Scheme 10 afforded the *syn*, as opposed to the *anti*, diastereomer. After all, 180° offset the binding modes for the aldehyde and imine!

Ellman proposed that their *syn* product resulted from an (E)-enolate that proceeded through a Zimmerman-Traxler chair-like transition state (Figure 3).[12] On the other hand, Scheme 10 predicted that a Zimmerman-Traxler chair-like transition state (**46**) afforded the *anti* product. To rationalize this apparent contradiction, it was necessary to recall that, unlike Ellman, the monodentate enolate in Scheme 10 adopted the (Z)-, as opposed to (E)-, conformation. Hence, the opposite diastereomer would have been expected!

Despite the *anti* selectivity, it was predicted that the bidentate chelated enolate (**43**) predominated at equilibrium due to its stronger Ti-O, in place of a Ti-Cl, bond. Therefore, the observed *anti* selectivity was rationalized by the higher steric requirement of the more crowded bicyclic boat (**45**), as opposed to chair (**46**), transition state. The increased *anti* selectivity for the more bulky **40aw** and **40ax** imines, along with their similar diastereomeric product ratios, further supported this steric, as opposed to electronic, argument.

Based on Scheme 10, three hypotheses were made as to how the diastereomeric product ratio could be changed. First, as a result of the steric hindrance between the ester and R^1 substituent in the Zimmerman-Traxler chair-like transition state (**46**), more of the *syn* product would be observed as the size of the ester increased. Second, as the lewis basicity of the ether oxygen increased, more of the *syn* product would be observed. Lewis basicity refers to the electron donating ability of an atom. Therefore, as the lewis basicity of the ether oxygen increased, more of the *syn* product would be observed due to the stabilization of the chelated enolate (**43**) and resulting bicyclic boat transition state (**45**). Third, in Scheme 10, the *two* diastereomers resulted from *two* structurally and *energetically* different transition states. Therefore, by altering the temperature of the enolate addition, the populations of the *two* transition states would be affected differently, and the diastereomeric product ratio would change.

Results

Barkin showed that when both the R^1 and R^2 substituents of the imine were aromatic, the *anti* diastereomer of the α-oxy-β-amino ester product predominated in all cases (Scheme 9). In addition to this data, it has recently been shown that by altering the lewis basicity of R^1, sterics of R^2, and the temperature at which the enolate addition was performed, the *anti:syn* (**50**:**51**) ratio of the products in Scheme 11 can be changed as depicted in Table 1.

Scheme 11

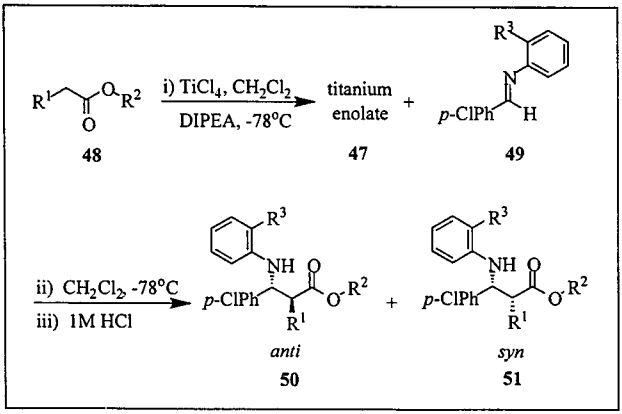

48 **47** **49** **50** **51**

Table 1: *anti:syn* (**50:51**) ratios for the α-oxy-β-amino ester products

Acetate	R^1	R^2	R^3	Imine	dr(**50:51**)[a]
48a	O*p*-NO_2Bn	Me	OMe	49a	90:10
48b	O*p*-ClBn	Me	OMe	49a	81:19
48c	OBn	Me	OMe	49a	65:35
48d	OBn	Me	OMe	49a	67:33[b]
48e	OMe	Me	OMe	49a	95:5[c]
48f	SMe	Me	OMe	49a	80:20[d]
48g	OH	Me	OMe	49a	53:47[e]
48h	OH	Me	OMe	49a	70:30[e,f]
48i	OMe	Et	OMe	49a	90:10
48j	OMe	*i*-Pr	OMe	49a	89:11
48k	OMe	Me	*i*-Pr	49b	95:5

[a] Determined by HPLC of crude mixture; [b] Reaction Conditions: 2x dilution; [c] Prepared and analyzed by Julia Barkin; [d] Verified by X-ray crystal structure of major diastereomer; [e] 2 equiv. of DIPEA were used; [f] Addition run at 0°C.

Based on the data in Table 1, five conclusions are clear. First, the diastereomeric ratios for the products from acetates **48a**, **48b** and **48c**, along with **48e**, **48f** and **48g**, revealed that as the electronegativity of the ether, or thioether, (R^1) decreased, an increase in the *syn* diastereomer was observed. The linear free energy relationship found for the products from acetates **48a**, **48b** and **48c** further supported this observation (Figure 6).

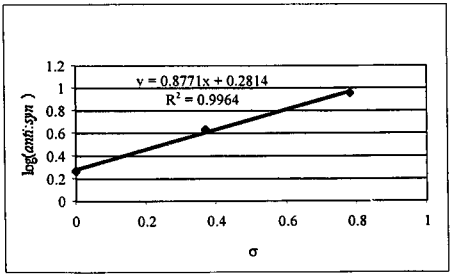

Figure 6. Plot of σ versus log (*anti:syn*)

Second, the diastereomeric product ratios from acetates **48c** and **48d** showed that a 2x-reaction dilution did not alter the *anti* selectivity. Third, the diastereomeric product ratios from acetates **48e**, **48i** and **48j** demonstrated that increasing the size of the ester (R^2) only produced slightly more of the *syn* product. Fourth, the diastereomeric product ratios from acetates **48e** and **48k** showed that further increasing the size of the *ortho* substituent of the imine (R^3) did not significantly affect the *anti* selectivity. Finally, the diastereomeric product ratios from acetates **48g** and **48h** demonstrated that performing the enolate addition at a higher temperature produced more of the *anti* diastereomer.

In addition to the experiments listed in Table 1, it is important to note some other key experiments that were attempted, but unsuccessful. For example, the methyl *p*-OCH_3, and *p*-Me benzyl substituted (R^1) acetates were synthesized along with the five phenolic analogues (*p*-NO_2, *p*-Cl, *p*-H, *p*-Me, *p*-OMe). Unfortunately, even though the *p*-Me substituted benzyl acetate, and *p*-OCH_3, *p*-Cl and *p*-Me substituted phenol acetates appeared to enolize, no addition was detected. Furthermore, the methyl *p*-OCH_3 benzyl acetate decomposed under the lewis acid reaction conditions as a result of its acid sensitivity. To alleviate this problem, a 1:1 $TiCl_4$:Ti(*i*-propoxide)$_4$ solution was prepared. Unfortunately, even though these milder conditions prevented decomposition, no addition was detected.

Attempts to investigate the steric effect of the ether substituent (R^1) were also unsuccessful. For example, while both the methyl OTBDMS and O*i*-Pr acetates were synthesized and appeared to enolize (Et_3N was used as the base for the OTBDMS acetate), no addition was detected.

Finally, to analyze nitrogen, a better lewis base as compared with oxygen or sulfur, the glycine methyl ester*HCl was enolized using three equivalents of base (DIPEA). Unfortunately, no enolization or addition appeared to have occurred.

In order to formulate the overall trends of Table 1, it was first necessary to determine the diastereomeric ratio for each product. This was accomplished using ^{1}H-NMR, HPLC and when possible X-ray crystallography. Figure 7 is the X-ray crystal structure of the major product from acetate **48f**.[13] This structure demonstrated that, in agreement with Barkin, the addition proceeded with *anti* selectivity!

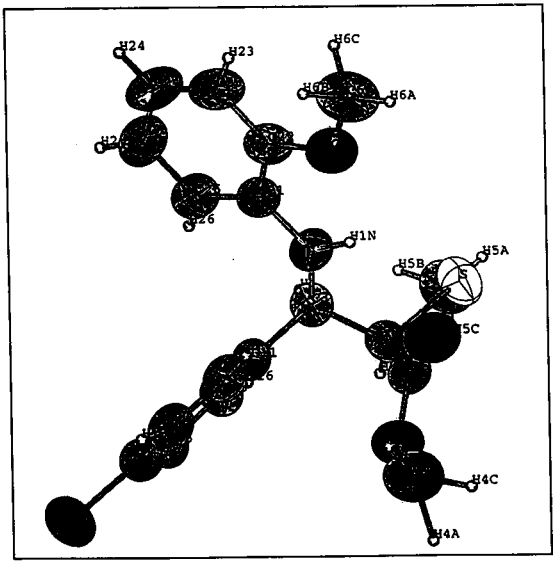

Figure 7. X-ray crystal structure of **50f**

After obtaining the crystal structure of **50f**, it was possible to calculate the diastereomeric product ratio for each addition by analogy using the ^{1}H-NMR and crude HPLC data. Figure 8 shows a section of the ^{1}H-NMR spectrum for the purified products from acetate **48h**.

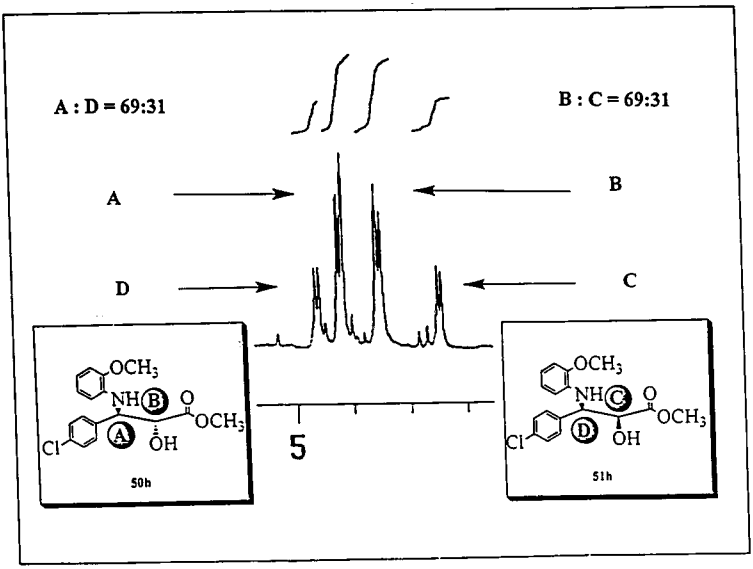

Figure 8. ^{1}H-NMR spectrum of **50h/51h**

The four doublets in Figure 8 corresponded to the α and β protons of the *anti* and *syn* diastereomeric products (**50h/51h**). By comparing Figure 8 with the NMR spectra of the other purified products (Appendix), it was clear that the β protons shifted the most downfield due to the deshielding nitrogen and phenyl ring. Furthermore, as a result of

the known selectivity, it was possible to assign the larger two doublets to the *anti* product, and calculate a diastereomeric product ratio of 69:31 from the peak integrations.

The diastereomeric product ratio was also determined using HPLC. Figure 9 is a section of the crude HPLC chromatogram for **50h/51h**.

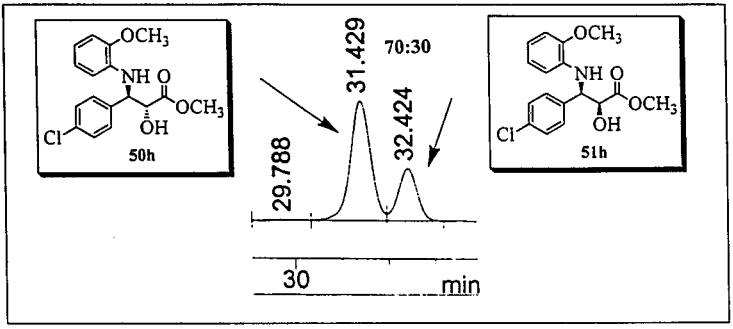

Figure 9. HPLC chromatogram for **50h/51h**

Based on the known selectivity, it was clear from Figure 9 that the *anti* diastereomer eluted before the *syn* product, and the diastereomeric product ratio equaled 70:30 (*anti*:*syn*).

Discussion

The results in Table 1 supported the three hypotheses made in the Introduction, and added further support for the proposed model (Scheme 12).

Scheme 12

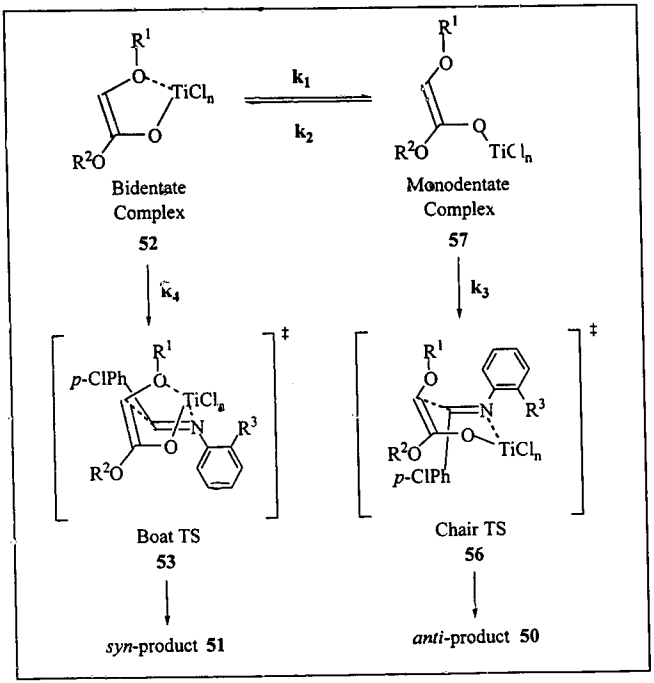

Table 1 showed that more of the *syn* product (**51**) was observed as the electronegativity of the R^1 substituent decreased: 90:10 (**50a:51a**), 81:19 (**50b:51b**), 65:35 (**50c:51c**) and 95:5 (**50e:51e**), 80:20 (**50f:51f**), 53:47 (**50g:51g**). By decreasing the

electronegativity of the R^1 substituent, the lewis basicity of the ether oxygen or sulfur increased, and the chelated enolate (**52**) and resulting bicyclic boat transition state (**53**) leading to the *syn* product (**51**) were stabilized.

Furthermore, Table 1 revealed that the diastereomeric product ratio did not change upon dilution; 65:35 (**50c**:**51c**), 67:33 (**50d**:**51d**). In addition to only needing *one* equivalent of lewis acid, this observation disfavored the possibility of ternary transition states **54** and **55** leading to the *syn* and *anti* products respectively.

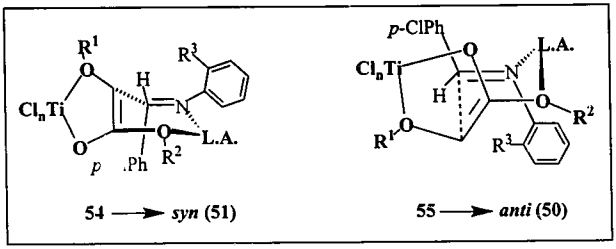

Figure 10. Ternary transition states

Likewise, Table 1 showed that as the size of the ester (R^2) increased, more of the *syn* product (**51**) was detected: 95:5 (**50e**:**51e**), 90:10 (**50i**:**51i**), 89:11 (**50j**:**51j**). Even though this change was not as large as expected, it was significantly outside the error range associated with the HPLC or NMR integrations, and was contributed to the destabilization of the Zimmerman-Traxler chair-like transition state (**56**).

Moreover, Table 1 demonstrated that the diastereomeric product ratio did not change upon further increasing the size of R^3: 95:5 (**50e**:**51e**), 95:5 (**50k**:**51k**). This implied that an *energetic* plateau prevented the diastereoselectivity from becoming >95:5 (*anti*:*syn*).

Finally, Table 1 demonstrated that more of the *anti* product was observed when the temperature of the enolate addition was raised: 53:47 (**50g:51g**), 70:30 (**50h:51h**). In Scheme 12, the *two* diastereomers resulted from *two* structurally and ***energetically*** different transition states. Consequently upon warming, the populations of the *two* transition states were not affected equally, and the diastereomeric product ratio was affected.

As was mentioned in the Introduction, it has been proposed that the bidentate chelated (Z)-enolate (**52**) predominated at equilibrium. That is,

$$K_{eq} = k_1 / k_2 = [57] / [52] < 1 \qquad 1$$

$$[57] = K_{eq} * [52] \qquad 2$$

Although, in order to rationalize the observed *anti* selectivity (Table 1), it has been proposed that an enolate pre-equilibrium exists, and $k_3 >>> k_4$. These presumptions are represented in Figure 11.

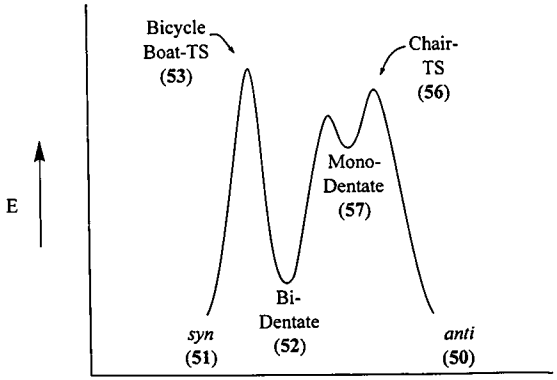

Figure 11. Proposed energy diagram

If it is assumed that enolate formation is *fast*, a pre-equilibrium develops between the bidentate enolate (**52**) and monodentate complex (**57**). Consequently, the assumption that $k_3 >>> k_4$ implies that the energy of activation leading to the bicyclic boat transition state (**53**) is much greater than that leading to the Zimmerman-Traxler chair-like transition state (**56**). This seemed plausible since (**53**) was more crowded than (**56**).

Furthermore, based on the assumptions that enolate formation is *fast* and $k_3 >>> k_4$, it may be concluded that the monodentate enolate (**57**) existed at a steady state concentration. After all, as a result of the low activation energy leading to the *anti* product (**50**), the small amount of monodentate enolate (**57**) present at equilibrium never accumulates. Using this pre-equilibrium, it is also possible to algebraically demonstrate that $k_3 >>> k_4$.

Equations **1** and **2** show that when a pre-equilibrium exists between **57** and **52**, k_3 and k_4 are the rate determining steps for Scheme 12.

$$\frac{dx}{dt} = \frac{\delta\, anti}{\delta\, t} = k_3 * [57] \qquad 3$$

$$\frac{dx}{dt} = \frac{\delta\, syn}{\delta t} = k_4 * [52] \qquad 4$$

In order to derive that $k_3 >>> k_4$, it is necessary to recall that the *anti*:*syn* product ratio from acetate **48g** ≈ 50:50. Consequently, we may conclude that $k_3 = k_4$ at –80°C, and equations **3** and **4** may be rewritten as shown.

$$k_3 * [57] = k_4 * [52] \qquad 5$$

Substituting **2** into **5** becomes:

$$k_3 * (K_{eq} * [\mathbf{52}]) = k_4 * [\mathbf{52}] \qquad \mathbf{6}$$

$$k_3 * K_{eq} = k_4 \qquad \mathbf{7}$$

Finally, since **1** assumed that $K_{eq} < 1$, **7** clearly demonstrated that $k_3 >>> k_4$.

Conclusion

We have shown that the titanium enolates (**47**) of α-alkoxy acetate esters (**48**) add cleanly to imines (**49**), and predominantly afford the *anti* diastereomer of the α-oxy-β-amino ester product (**50**). In order to rationalize this selectivity, we proposed the model in Scheme 12. In support of this model, it was shown that more of the *syn* product was observed when the electronegativity of the ether or thio ether (R^1) decreased, and the size of the ester (R^2) increased. Furthermore, since more of the *anti* product was observed when the temperature of the enolate addition was raised, it was concluded that the activation energy leading to the *syn* product was much greater than that leading to the *anti* diastereomer.

Future Work

We have shown that when R^1=OH, a temperature increase produced more of the *anti* diastereomer: 53:47 (**50g**:**51g**), 70:30 (**50h**:**51h**). To further verify and determine the limit of this selectivity change, all of the additions in Table 1 should be performed at both 0°C and higher temperatures.

Furthermore, we demonstrated that the *diastereoselectivity* of our imine-aldol addition could be controlled. By using *chiral* imines, it may also be possible to induce *enantioselective* control in the products.

Experimental

General. Unless otherwise noted, all reactions were run under N_2. Solvents were distilled by the following drying agents: dichloromethane (CH_2Cl_2) from CaH_2, and tetrahydrofuran (THF) from sodium. Thin Layer Chromatography (TLC) was performed using E. Merck silica gel 60 Å (0.25 mm) analytical glass plates. E. Merck silica gel 60 Å (200-425 mesh) was used to perform column chromatography according to the method of Still.[14] Melting points were determined on a Mel-temp II® capillary melting point apparatus, and are uncorrected. ^{1}H-NMR and ^{13}C-NMR were obtained in $CDCl_3$ at 200 MHz and 50 MHz respectively on a Varian Gemini 2200 Spectrometer. The following conventions were used in interpreting the ^{1}H-NMR spectra: s=singlet, bs=broad singlet, d=doublet, dd=doublet of doublets, t=triplet, bt=broad triplet, td=triplet of doublets and m=multiplet. IR were obtained on a Perkin Elmer 1600 series FTIR spectrometer. HPLC data of the crude samples were obtained on a Hewlett Packard 1100 series HPLC, using a Zorbax SB-C18 4.6 mm x 25 cm column. Unless noted otherwise, the following elution gradient was used: an CH_3CN:H_2O mixture was varied over 13 minutes from 60:40 to 80:20, and run for 20 minutes at a flow rate of 1mL/min.

N-(2-methoxyphenyl)-4-chlorobenzaldimine (49a). To a stirred solution of *o*-anisdine (2.85 g, 23.1 mmol) and *p*-chlorobenzaldehyde (3.24 g, 23.0 mmol) in 30.0 mL of toluene at rt was added approximately 2 g of 4 Å mol. Sieves. After 24 h, the resulting mixture was filtered and concentrated *in vacuo*. The resulting solid was recrystallized from ethanol (50.0 mL) to afford 10.38 g (82 %) as yellow plates, mp=76-78°C. R_f=0.16 (SiO_2 15% EtAc/Hex). 200 MHz ^{1}H-NMR ($CDCl_3$) δ 8.44 (s, 1H), 7.86 (d, 2H, J=8.4 Hz), 7.43 (d, 2H, J=8.4 Hz), 7.20 (m, 1H), 6.99 (m, 3H), 3.88 (s, 3H). 50 MHz ^{13}C-NMR

($CDCl_3$) δ 159.79, 152.27, 141.39, 137.25, 130.06, 128.98, 126.97, 121.07, 120.29, 111.55, 55.85. IR (neat) 3059, 3001, 2945, 2845, 1624, 1584, 1486, 1245, 1100, 1028, 846, 821, 745 cm^{-1}.

N-(2-isopropylphenyl)-4-chlorobenzaldimine (49b). To a stirred solution of 2-isopropyl aniline (2.70 g, 20.0 mmol) and *p*-chlorobenzaldehyde (2.81 g, 20.0 mmol) in 30.0 mL of toluene at rt was added approximately 2 g of 4 Å mol. Sieves. After 24 h, the resulting mixture was filtered and concentrated *in vacuo*. The resulting solid was recrystallized from ethanol (50.0 mL) to afford 0.76 g (14 %) as yellow fibers, mp=44-46°C. R_f=0.69 (SiO_2 15% EtAc/Hex). 200 MHz ^{1}H-NMR ($CDCl_3$) δ 8.34 (s, 1H), 7.86 (d, 2H, J=8.4 Hz), 7.46 (d, 2H, J=8.4 Hz), 7.27 (m, 3H), 6.90 (t, 1H, J=5.2 Hz, 3.6 Hz), 3.50 (m, 1H, J=6.8 Hz), 1.23 (d, 6H, J=7.0 Hz). 50 MHz ^{13}C-NMR ($CDCl_3$) δ 157.75, 149.62, 142.33, 135.05, 129.88, 129.04, 126.55, 126.26, 125.58, 117.62, 96.98, 28.16, 23.11. IR (neat) 3047, 3000, 2944, 2840, 1629, 1486, 1079, 821, 747 cm^{-1}.

Methyl oxy-4-nitrobenzyl acetate (48a). To a stirred suspension of NaH (0.79 g, 19.7 mmol, washed with hexanes) in THF (10.0 mL), was added dropwise a solution of *p*-nitrobenzyl alcohol (2.90 g, 19.0 mmol), and methyl bromoacetate (1.8 mL, 19.7 mmol) in THF (12.0 mL). After 3 h, the red mixture was poured into 75.0 mL of water, and extracted with 2 x 75.0 mL portions of CH_2Cl_2. The combined organic phases were then washed with 5 x 50.0 mL portions of water, 50.0 mL of brine, dried ($MgSO_4$), filtered and concentrated *in vacuo*. The resulting solid was recrystallized from ethanol to afford 2.62 g (61%) as yellow plates, mp=72-74°C. R_f=0.22 (SiO_2 15% EtAc/Hex). 200 MHz ^{1}H-NMR ($CDCl_3$) δ 8.23 (d, 2H, J=9.0 Hz), 7.55 (d, 2H, J=9.0 Hz), 4.74 (s, 2H), 4.20 (s, 2H), 3.97 (s, 3H). 50 MHz ^{13}C-NMR ($CDCl_3$) δ 170.35, 144.79, 127.95, 123.66,

72.04, 67.71, 51.98. IR (neat) 3116, 2920, 1744, 1619, 1544, 1330, 1217, 1137, 839, 730 cm^{-1}.

Methyl 3-(2-methoxyphenyl)amino-2-(4-nitrobenzoxy)-3-(4-chlorophenyl) propanoate (50a/51a). To a stirred solution of **48a** (0.45 g, 2.0 mmol) in CH_2Cl_2 (15.0 mL) cooled to –78°C was added dropwise a 1 M solution of $TiCl_4$ in CH_2Cl_2 (2.2 mL, 2.2 mmol). After 5 minutes of precomplexing, DIPEA (400 µL, 2.3 mmol) was added dropwise. After 30 minutes of stirring, this violet solution was transferred *via cannula* to a solution of **49a** (0.248 g, 1.0 mmol) in CH_2Cl_2 (8.0 mL) also at –78°C. The resulting solution was quenched after 2 h by the addition of 15.0 mL of 1 M HCl. The organic phase was separated. washed with brine (25.0 mL), dried ($MgSO_4$), filtered and concentrated *in vacuo*. The resulting brown oil was purified by flash chromatography to afford 0.15 g (66 %) of an orange oil. R_f=0.52 (SiO_2 10% Hex/CH_2Cl_2). 200 MHz ^{1}H-NMR ($CDCl_3$) δ 8.18 (d, 2H, J=8.8 Hz), 7.44 (d, 2H, J=8.8 Hz), 7.28 (s, 4H), 6.70 (m, 3H), 6.43 (dd, 1H, J=1.8 Hz, 7.4 Hz), 6.29 (***syn* isomer**, m, 1H), 5.24 (bs, 1H), 3.89 (***syn* isomer**, s, 3H), 3.87 (s, 3H), 3.76 (***syn* isomer**, s, 3H), 3.70 (s, 3H). 50 MHz ^{13}C-NMR ($CDCl_3$) δ 170.37, 147.07, 144.52, 136.75, 135.49, 133.73, 128.62, 128.52, 128.06, 123.62, 121.10, 120.95 (***syn* isomer**), 117.70, 117.41 (***syn* isomer**), 111.25, 109.63, 81.92 (***syn* isomer**), 80.85, 71.71, 58.67 (***syn* isomer**), 58.35, 55.54, 52.51 (***syn* isomer**), 52.23, 29.70. IR (neat) 3425, 2943, 1750, 1610, 1520, 1390, 1216, 1130, 839, 735 cm^{-1}. HPLC 88:12 *anti:syn*.

Methyl oxy-4-chlorobenzyl acetate (48b). To a stirred suspension of NaH (0.79 g, 19.7 mmol, washed with hexanes) in THF (15.0 mL), was added dropwise a solution of *p*-chlorobenzyl alcohol (2.71 g, 19.0 mmol), and methyl bromoacetate (2.98 g, 19.5

mmol) in THF (10.0 mL). After 4 h, the orange mixture was poured into 75.0 mL of water, and extracted with 2 x 75.0 mL portions of CH_2Cl_2. The combined organic phases were then washed with 8 x 75.0 mL portions of water, 50.0 mL of brine, dried ($MgSO_4$), filtered and concentrated *in vacuo* to afford 3.33 g (82%) of a yellow oil. R_f=0.20 (SiO_2 15% EtAc/Hex). 200 MHz ^{1}H-NMR ($CDCl_3$) δ 7.32 (s, 4H), 4.59 (s, 2H), 4.11 (s, 2H), 3.77 (s, 3H). 50 MHz ^{13}C-NMR ($CDCl_3$) δ 170.62, 135.67, 128.73, 128.55, 128.12, 72.40, 67.10, 51.79. IR (neat) 2954, 2872, 1749, 1510, 1210, 1128, 1010, 805 cm^{-1}.

Methyl 3-(2-methoxyphenyl)amino-2-(4-chlorobenzoxy)-3-(4-chlorophenyl) propanoate (50b/51b). To a stirred solution of **48b** (0.21 g, 1.0 mmol) in CH_2Cl_2 (12.0 mL) cooled to –78°C was added dropwise a 1 M solution of $TiCl_4$ in CH_2Cl_2 (1.2 mL, 1.2 mmol). After 5 minutes of precomplexing, DIPEA (226 μL, 1.3 mmol) was added dropwise. After 30 minutes of stirring, this violet solution was transferred *via cannula* to a solution of **49a** (0.37 g, 1.5 mmol) in CH_2Cl_2 (8.0 mL) also at –78°C. The resulting solution was quenched after 2 h by the addition of 15.0 mL of 1 M HCl. The organic phase was separated, washed with brine (25.0 mL), dried ($MgSO_4$), filtered and concentrated *in vacuo*. The resulting brown oil was purified by flash chromatography to afford 0.15 g (32 % based on crude ^{1}H-NMR) of a green oil. R_f=0.21 (SiO_2 50% Hex/CH_2Cl_2). 200 MHz ^{1}H-NMR ($CDCl_3$) δ 7.26 (m, 8H), 6.70 (m, 3H), 6.40 (dd, 1H, J=1.8 Hz, 7.4 Hz), 6.26 (***syn* isomer**, dd, 1H, J=9.2 Hz), 4.82 (d, 1H, J=5.2 Hz), 4.36 (d, 1H, J=5.6 Hz), 4.32 (s, 2H), 3.88 (***syn* isomer**, s, 3H), 3.86 (s, 3H), 3.73 (***syn* isomer**, s, 3H), 3.68 (s, 3H). 50 MHz ^{13}C-NMR ($CDCl_3$) δ 170.64, 147.06, 136.96, 135.56, 135.40 (***syn* isomer**), 133.80, 133.56 (***syn* isomer**), 129.34, 128.68, 128.53, 121.05, 117.50, 111.33, 109.55, 80.96 (***syn* isomer**), 80.43, 72.54, 58.69 (***syn* isomer**), 58.29, 55.50,

51.95, 29.71. IR (neat) 3414, 2945, 2910, 1750, 1510, 1219, 1131, 1024, 804, 735 cm^{-1}. HPLC 81:19 *anti:syn*.

Methyl oxy-benzyl acetate (48c/d). To a stirred suspension of KH (2.44 g, 61.0 mmol, washed with hexanes) in dry DMF (50.0 mL), was added dropwise a solution of methyl glycolate (5.00 g, 55.5 mmol), and benzyl bromide (7.26 mL, 61.0 mmol) in dry DMF (10.0 mL). After 2 h, the orange mixture was poured into 100.0 mL of water, and extracted with 2 x 100.0 mL portions of CH_2Cl_2. The combined organic phases were then washed with 10 x 100.0 mL portions of water, 50.0 mL of brine, dried ($MgSO_4$), filtered and concentrated *in vacuo*. The resulting yellow oil was purified by column chromatography to afford 2.25 g (25%) of an orange oil. R_f=0.19 (SiO_2 50% Hex/CH_2Cl_2). 200 MHz ^{1}H-NMR ($CDCl_3$) δ 7.36 (bs, 5H), 4.63 (s, 2H), 4.11 (s, 2H), 3.76 (s, 3H). 50 MHz ^{13}C-NMR ($CDCl_3$) δ 170.80, 137.18, 128.61, 128.49, 72.91, 67.12, 51.73, 39.30. IR (neat) 3026, 2954, 1749, 1449, 1210, 1123, 744, 692 cm^{-1}.

Methyl-3-(2-methoxyphenyl)amino-2-benzoxy-3-(4-chlorophenyl) propanoate (50c/51c). To a stirred solution of **48c/d** (0.36 g, 2.0 mmol) in CH_2Cl_2 (6.0 mL) cooled to –78°C was added dropwise a 1 M solution of $TiCl_4$ in CH_2Cl_2 (2.2 mL, 2.2 mmol). After 5 minutes of precomplexing, DIPEA (400 μL, 2.3 mmol) was added dropwise. After 1 h of stirring, this violet solution was transferred *via cannula* to a solution of **49a** (0.249 g, 1.0 mmol) in CH_2Cl_2 (4.0 mL) also at –78°C. The resulting solution was quenched after 2 h by the addition of 15.0 mL of 1 M HCl. The organic phase was separated, washed with brine (25.0 mL), dried ($MgSO_4$), filtered and concentrated *in vacuo*. The resulting brown oil was purified by column chromatography to afford 0.12 g (66%) of an orange oil. R_f=0.28 (SiO_2 55% Hex/CH_2Cl_2). 200 MHz ^{1}H-NMR ($CDCl_3$) δ

7.22 (m, 9H), 6.66 (m, 3H), 6.37 (dd, 1H, J=2.2 Hz, 7.4 Hz), 6.25 (***syn* isomer**, m, 1H), 4.87 (***syn* isomer**, t, 1H, J=6.0 Hz), 4.80 (t, 1H, J=5.6 Hz), 3.86 (***syn* isomer**, s, 3H), 3.85 (s, 3H), 3.71 (***syn* isomer**, s, 3H), 3.66 (s, 3H). 50 MHz ^{13}C-NMR ($CDCl_3$) δ 170.87, 147.09, 136.90, 136.62 (***syn* isomer**), 133.48, 133.11 (***syn* isomer**), 129.12, 128.51, 128.32, 121.05, 120.93 (***syn* isomer**), 117.35, 117.14 (***syn* isomer**), 111.31, 111.19 (***syn* isomer**), 109.55, 80.86 (***syn* isomer**), 80.48, 73.02, 72.46 (***syn* isomer**), 66.97, 66.62 (***syn* isomer**), 58.78 (***syn* isomer**), 58.35, 55.50, 52.32 (***syn* isomer**), 52.07, 39.38, 29.74. IR (neat) 3414, 3036, 2921, 1750, 1610, 1537, 1476, 1217, 1128, 735, 695 cm^{-1}. HPLC 65:35 *anti:syn*.

Methyl-3-(2-methoxyphenyl)amino-2-benzoxy-3-(4-chlorophenyl) propanoate (50d/51d). To a stirred solution of **48c/d** (0.45 g, 2.5 mmol) in CH_2Cl_2 (12.0 mL) cooled to –78°C was added dropwise a 1 M solution of $TiCl_4$ in CH_2Cl_2 (2.2 mL, 2.2 mmol). After 5 minutes of precomplexing, DIPEA (400 μL, 2.3 mmol) was added dropwise. After 30 min. of stirring, this violet solution was transferred *via cannula* to a solution of **49a** (0.249 g, 1.0 mmol) in CH_2Cl_2 (8.0 mL) also at –78°C. The resulting solution was quenched after 2 h by the addition of 15.0 mL of 1 M HCl. The organic phase was separated, washed with brine (25.0 mL), dried ($MgSO_4$), filtered and concentrated *in vacuo*. The resulting yellow oil was purified by column chromatography to afford 0.160 g (38 %) of an orange oil. R_f=0.20 (SiO_2 60% Hex/CH_2Cl_2). 200 MHz ^{1}H-NMR ($CDCl_3$) δ 7.22 (m, 9H), 6.66 (m, 3H), 6.37 (dd, 1H, J=2.2 Hz, 7.4 Hz), 6.25 (***syn* isomer**, m, 1H), 4.87 (***syn* isomer**, t, 1H, J=6.0 Hz), 4.80 (t, 1H, J=5.6 Hz), 3.86 (***syn* isomer**, s, 3H), 3.85 (s, 3H), 3.71 (***syn* isomer**, s, 3H), 3.66 (s, 3H). 50 MHz ^{13}C-NMR ($CDCl_3$) δ 170.87, 147.09, 136.90, 136.62 (***syn* isomer**), 133.48, 133.11 (***syn***

isomer), 129.12, 128.51, 128.32, 121.05, 120.93 (***syn* isomer**), 117.35, 117.14 (***syn* isomer**), 111.31, 111.19 (***syn* isomer**), 109.55, 80.86 (***syn* isomer**), 80.48, 73.02, 72.46 (***syn* isomer**), 66.97, 66.62 (***syn* isomer**), 58.78 (***syn* isomer**), 58.35, 55.50, 52.32 (***syn* isomer**), 52.07, 39.38, 29.74. IR (neat) 3414, 3036, 2921, 1750, 1610, 1537, 1476, 1217, 1128, 735, 695 cm^{-1}. HPLC 67:33 *anti:syn.*

Methyl-3-(2-methoxyphenyl)amino-2-methylthio-3-(4-chlorophenyl) propanoate (50f/51f). To a stirred solution of **48f** (0.124 g, 1.0 mmol) in CH_2Cl_2 (5.0 mL) cooled to –78°C was added dropwise a 1 M solution of $TiCl_4$ in CH_2Cl_2 (1.2 mL, 1.2 mmol). After 5 minutes of precomplexing, DIPEA (230 μL, 1.3 mmol) was added dropwise. After 1 h of stirring, this violet solution was transferred *via cannula* to a solution of **49a** (0.37 g, 1.5 mmol) in CH_2Cl_2 (7.0 mL) also at –78°C. The resulting solution was quenched after 2 h by the addition of 15.0 mL of 1 M HCl. The organic phase was separated, washed with brine (25.0 mL), dried ($MgSO_4$), filtered and concentrated *in vacuo*. The resulting solid was filtered with cold ethanol to afford 0.14 g (38%) as white cubes, mp=100-101°C. R_f=0.16 (SiO_2 50%Hex/CH_2Cl_2). 200 MHz ^{1}H-NMR ($CDCl_3$) ***anti* isomer** δ 7.26 (s, 4H), 6.74 (m, 3H), 6.40 (d, 1H, J= 9.0 Hz), 5.53 (d, 1H, J=9.0 Hz), 4.84 (t, 1H, J= 8.0 Hz), 3.87 (s, 3H), 3.68 (s, 3H), 3.62 (d, 1H, J=7.0 Hz), 2.11 (s, 3H). 50 MHz ^{13}C-NMR ($CDCl_3$) ***anti* isomer** δ 171.40, 147.07, 138.54, 136.07, 133.49, 128.78, 128.27, 121.04, 117.33, 111.14, 109.69, 58.61, 55.64, 54.65, 52.42, 15.63. IR (neat) 3402, 2921, 2841, 1727, 1612, 1562, 1245, 1154, 821, 735 cm^{-1}. HPLC 80:20 *anti:syn.*

Methyl 3-(2-methoxyphenyl)amino-2-hydroxy-3-(4-chlorophenyl) propanoate (50g/51g). To a stirred solution of **48g/h** (0.180 g, 2.0 mmol) in CH_2Cl_2 (8.0 mL) cooled to –78°C was added dropwise a 1 M solution of $TiCl_4$ in CH_2Cl_2 (2.2 mL, 2.2 mmol).

After 5 minutes of precomplexing, DIPEA (0.80 mL, 4.6 mmol) was added dropwise. After 1 h of stirring, this violet solution was transferred *via cannula* to a solution of **49a** (0.249 g, 1.0 mmol) in CH_2Cl_2 (4.0 mL) also at –78°C. The resulting solution was quenched after 2 h by the addition of 15.0 mL of 1 M HCl. The organic phase was separated, washed with brine (25.0 mL), dried ($MgSO_4$), filtered and concentrated *in vacuo*. The resulting yellow oil was purified by column chromatography to afford 0.042 g (12 %) of a yellow oil. R_f=0.36 (SiO_2 5% ether/CH_2Cl_2). 200 MHz ^{1}H-NMR ($CDCl_3$) δ 7.26 (m, 4H), 6.75 (m, 3H), 6.38 (d, 1H, J=7.4 Hz), 5.40 (d, 1H, J=8.0 Hz), 5.27 (d, 1H, J=8.2 Hz), 4.92 (d, 1H, J=3.0 Hz), 4.84 (d, 1H, J=3.6 Hz), 4.70 (d, 1H, J=3.6 Hz), 4.49 (d, 1H, J=2.6 Hz), 3.89 (s, 3H), 3.87 (s, 3H), 3.79 (s, 3H), 3.75 (s, 3H). 50 MHz ^{13}C-NMR ($CDCl_3$) δ 173.11, 147.21, 137.95, 135.60, 128.73, 128.34, 120.98, 118.55, 117.45, 111.58, 111.26, 109.70, 74.44, 73.53, 58.86, 58.36, 53.12, 29.67. IR (neat) 3414, 2921, 2852, 1738.3, 1612, 1535, 1223, 1108, 735 cm^{-1}. The HPLC eluant gradient was varied over 18 minutes from 35:65 to 45:55 CH_3CN:H_2O, and run for 30 minutes at a flow rate of 1mL/min., 53:47 *anti:syn*.

Methyl 3-(2-methoxyphenyl)amino-2-hydroxy-3-(4-chlorophenyl) propanoate (50h/51h). To a stirred solution of **48g/h** (0.180 g, 2.0 mmol) in CH_2Cl_2 (8.0 mL) cooled to –78°C was added dropwise a 1 M solution of $TiCl_4$ in CH_2Cl_2 (2.2 mL, 2.2 mmol). After 5 minutes of precomplexing, DIPEA (0.80 mL, 4.6 mmol) was added dropwise. After 1 h of stirring, this violet solution was transferred *via cannula* to a solution of **49a** (0.249 g, 1.0 mmol) in CH_2Cl_2 (4.0 mL) at 0°C. The resulting solution was quenched after 2 h by the addition of 15.0 mL of 1 M HCl. The organic phase was separated, washed with brine (25.0 mL), dried ($MgSO_4$), filtered and concentrated *in*

vacuo. The resulting yellow oil was purified by column chromatography to afford 0.07 g (20 %) of a yellow oil. R_f=0.36 (SiO_2 5% ether/CH_2Cl_2). 200 MHz ^{1}H-NMR ($CDCl_3$) δ 7.26 (m, 4H), 6.75 (m, 3H), 6.38 (d. 1H, J=6.0 Hz), 4.92 (***syn* isomer**, d, 1H, J=3.0 Hz), 4.84 (d, 1H, J=3.0 Hz), 4.71 (d, 1H, J=3.0 Hz), 4.49 (***syn* isomer**, d, 1H. J=3.0 Hz), 3.89 (s, 3H), 3.82 (***syn* isomer**, s, 3H), 3.79 (***syn* isomer**, s, 3H), 3.75 (s, 3H). 50 MHz ^{13}C-NMR ($CDCl_3$) δ 173.11, 147.15, 137.90, 135.62, 131.60, 128.74, 128.35, 122.07 (***syn* isomer**), 121.04, 118.47 (***syn* isomer**), 117.47, 111.63 (***syn* isomer**), 111.26, 109.54, 74.46 (***syn* isomer**), 73.51, 62.88, 58.80, 58.28 (***syn* isomer**), 55.47, 52.69, 29.70. IR (neat) 3414, 2921, 2852, 1738.3, 1612, 1535, 1223, 1108, 735 cm^{-1}. The HPLC eluant gradient was varied over 18 minutes from 35:65 to 45:55 CH_3CN:H_2O, and run for 30 minutes at a flow rate of 1mL/min., 70:30 *anti:syn*.

Ethyl methoxy acetate (48i). A stirred solution of methoxyacetic acid (1.82 g, 20.0 mmol), conc. H_2SO_4 (cat), and 25.0 mL of 95% ethanol equipped with a drying tube was refluxed overnight in an oil bath, and distilled using a cow-arm extension at 140°C to collect 2.28 g (96%) of a yellow oil. R_f=0.55 (SiO_2 15% EtAc/Hex). 200 MHz ^{1}H-NMR ($CDCl_3$) δ 4.24 (m, 2H, J=7.0 Hz), 4.03 (s, 2H), 3.45 (s, 3H), 1.30 (t, 3H, J=7.0 Hz). 50 MHz ^{13}C-NMR ($CDCl_3$) δ 169.93, 69.42, 60.41, 58.82, 13.82. IR (neat) 2985, 1744, 1200, 1123, 720 cm^{-1}.

Ethyl-3-(2-methoxyphenyl)amino-2-methoxy-3-(4-chlorophenyl) propanoate (50i/51i). To a stirred solution of **48i** (0.118 g, 1.0 mmol) in CH_2Cl_2 (5.0 mL) cooled to –78°C was added dropwise a 1 M solution of $TiCl_4$ in CH_2Cl_2 (1.2 mL, 1.2 mmol). After 5 minutes of precomplexing, DIPEA (230 μL, 1.3 mmol) was added dropwise. After 1 h of stirring, this violet solution was transferred *via cannula* to a solution of **49a** (0.37 g,

1.5 mmol) in CH_2Cl_2 (11.0 mL) also at–78°C. The resulting solution was quenched after 2 h by the addition of 15.0 mL of 1 M HCl. The organic phase was separated, washed with brine (25.0 mL), dried ($MgSO_4$), filtered and concentrated *in vacuo*. The resulting yellow oil was purified by column chromatography to afford 0.027 g (10 %) of an orange oil. R_f=0.27 (SiO_2 50% Hex/CH_2Cl_2). 200 MHz ^{1}H-NMR ($CDCl_3$) δ 7.25 (s, 4H), 6.74 (m, 3H), 6.38 (dd, 1H, J=2.0 Hz, 7.0 Hz), 6.25 (***syn* isomer,** m, 1H), 5.30 (d, 1H), 4.79 (bt, 1H), 4.14 (m, 2H, J=7.4 Hz), 3.88 (s, 3H), 3.44 (s, 3H), 1.19 (t, 3H, J=7.4 Hz). Not enough product to obtain a 50 MHz ^{13}C-NMR spectra. IR (neat) 3414, 2921, 2841, 1744, 1595, 1509, 1452, 1217, 1126, 1022, 730 cm^{-1}. HPLC 90:10 *anti:syn*.

Isopropyl methoxy acetate (48j). A stirred solution of methoxyacetic acid (2.27 g, 25.0 mmol), conc. H_2SO_4 (cat), and 30.0 mL of isopropyl alcohol equipped with a drying tube was refluxed overnight in an oil bath. The resulting yellow mixture was poured into 25.0 mL of water, and extracted with 2 x 25.0 mL portions of CH_2Cl_2. The combined organic phases were then washed with 2 x 25.0 mL portions of sat. $NaHCO_3$, 2 x 25.0 mL portions of water, 25.0 mL of brine, dried ($MgSO_4$), filtered and concentrated *in vacuo* to afford 0.73 g (22%) of a yellow oil. . R_f=0.55 (SiO_2 15% EtAc/Hex). 200 MHz ^{1}H-NMR ($CDCl_3$) δ 5.12 (m, 1H, J=6.0 Hz), 3.99 (s, 2H), 3.45 (s, 3H), 1.27 (d, 6H, J=2.0 Hz). 50 MHz ^{13}C-NMR ($CDCl_3$) δ 169.56, 69.80, 68.18, 59.00, 21.57. IR (neat) 2974, 2900, 2810, 1739, 1200, 1118, 925, 718 cm^{-1}.

Isopropyl-3-(2-methoxyphenyl)amino-2-methoxy-3-(4-chlorophenyl) propanoate (50j/51j). To a stirred solution of **48j** (0.13 g, 1.0 mmol) in CH_2Cl_2 (5.0 mL) cooled to –78°C was added dropwise a 1 M solution of $TiCl_4$ in CH_2Cl_2 (1.2 mL, 1.2 mmol). After 5 minutes of precomplexing, DIPEA (230 μL, 1.3 mmol) was added dropwise. After 1 h

of stirring, this violet solution was transferred *via cannula* to a solution of **49a** (0.37 g, 1.5 mmol) in CH_2Cl_2 (7.0 mL) also at –78°C. The resulting solution was quenched after 2 h by the addition of 15.0 mL of 1 M HCl. The organic phase was separated, washed with brine (25.0 mL), dried ($MgSO_4$), filtered and concentrated *in vacuo*. The resulting yellow oil was purified by column chromatography to afford 0.029 g (8 %) of an orange oil. R_f=0.29 (SiO_2 50% Hex/CH_2Cl_2). 200 MHz ^{1}H-NMR ($CDCl_3$) δ 7.26 (m, 4H), 6.70 (m, 3H), 6.37 (dd, 1H, J=2.0 Hz, 7.0 Hz), 6.27 (***syn* isomer**, dd, 1H), 5.30 (bs, 1H), 5.01 (m, 1H, J=6.0 Hz), 4.77 (bs, 1H), 4.09 (d, 1H, J=5.0 Hz), 3.88 (s, 3H), 3.42 (s, 3H), 1.17 (t, 6H, J=6.2 Hz). 50 MHz ^{13}C-NMR ($CDCl_3$) δ 171.40, 148.09, 137.98, 133.62, 131.50, 128.63, 128.49, 124.12, 121.22, 119.85, 109.92, 71.68, 69.06, 55.81, 29.69, 21.49. IR (neat) 3414, 2978, 2910, 1738, 1623, 1540, 1223, 1102, 735 cm^{-1}. HPLC 89:11 *anti:syn*.

Methyl 3-(2-isopropylphenyl)amino-2-(methoxy)-3-(4-chlorophenyl) propanoate (50k/51k). To a stirred solution of **48k** (0.10 g, 1.0 mmol) in CH_2Cl_2 (12.0 mL) cooled to –78°C was added dropwise a 1 M solution of $TiCl_4$ in CH_2Cl_2 (1.2 mL, 1.2 mmol). After 5 minutes of precomplexing, DIPEA (226 μL, 1.3 mmol) was added dropwise. After 30 minutes of stirring, this violet solution was transferred *via cannula* to a solution of **49b** (0.35 g, 1.35 mmol) in CH_2Cl_2 (8.0 mL) also at –78°C. The resulting solution was quenched after 2 h by the addition of 15.0 mL of 1 M HCl. The organic phase was separated, washed with brine (25.0 mL), dried ($MgSO_4$), filtered and concentrated *in vacuo*. The resulting brown oil was purified by flash chromatography to afford 0.04 g (11 %) of a brown oil. R_f=0.25 (SiO_2 40% Hex/CH_2Cl_2). 200 MHz ^{1}H-NMR ($CDCl_3$) δ 7.26 (s, 4H), 7.14 (dd, 1H, J=1.6 Hz, 7.8 Hz), 6.94 (td, 1H, J=1.4 Hz, 7.6 Hz), 6.71 (td, 1H, J=1.2 Hz, 7.2 Hz), 6.35 (dd, 1H, J=1.2 Hz, 8.0 Hz), 4.90 (bs, 1H),

4.82 (t, 1H, J=4.8 Hz), 4.17 (d, 1H, J=4.4 Hz), 3.72 (***syn* isomer**, s, 3H), 3.65 (s, 3H), 3.44 (s, 3H), 3.45 (***syn* isomer**, s, 3H), 3.00 (m, 1H, J=6.6 Hz), 1.32 (d, 6H, J=6.6 Hz). 50 MHz ^{13}C-NMR ($CDCl_3$) δ 170.50, 157.80, 137.04, 133.53, 132.74, 129.89, 129.04, 128.68, 126.54, 125.12, 117.99, 111.72, 83.39, 58.67, 52.22, 27.55, 22.19. IR (neat) 3425, 3059, 2955, 1738, 1584, 1509, 1492, 1446, 1200, 1125, 1085, 827, 745 cm^{-1}. HPLC 95:5 *anti:syn*.

References

(1) Ojima, I.; Habus, I.; Zhao, M.; Zucco, M.; Park, Y. H.; Sun, C. M.; Brigaud, T. *Tetrahedron*. **1992**, *48*, 6985-7012.

(2) Nicolaou, K. C.; Yang, Z.; Liu, J. J.; Ueno, H.; Nantermet, P. G.; Guy, R. K.; Claiborne, C. F.; Renaud, J.; Couladouros, E. A.; Paulvannan, K.; Sorenson, E. J. *Nature*. **1994**, *367*, 630.

(3) Holton, R. A.; Kim, H-B.; Somoza, C.; Liang, F;, Biediger, R. J.; Boatman, P. D.; Shindo, M.; Smith, C. C.; Kim, S.; Nadizadeh, H.; Suzuki, Y.; Tao, C.; Vu, P.; Tang, S.; Zhang, P.; Murthi, K. K.; Gentile, L. N.; Liu, J. H. *J. Am. Chem. Soc.* **1994**, *116*, 1599.

(4) Kanazawa, A. M.; Denis, J-N.; Greene, A. *J. Chem. Soc. Chem. Commun.* **1994**, 2591-2592.

(5) Tamariz, J. Biological Activity of b-Amino Acids and b-Lactams. In *Enantioselective Synthesis of b-Amino Acids*. Juaristi, E. Wiley-VCH, Inc. New York, **1996**. 1-43 and references cited there-in.

(6) Evans, D.A.; Urpí, F.; Somers, T.C.; Clark, J.S.; Bilodeau, M.T. *J. Am. Chem. Soc.* **1990**, *112*, 8215-8216.

(7) Figueras, S.; Martín, R.; Romea, P.; Urpí, F.; Vilarrasa, J. *Tetrahedron Lett.* **1997**, *38*, 1637-1640.

(8) Annunziata, R.; Cinquini, M.; Cozzi, F.; Borgia, A. L. *J. Org. Chem.* **1992**. *57*, 6339-6342.

(9) Mukai, C.; Kim, I.J.; Furu, E.; Hanaoka, M. *Tetrahedron*. **1993**, *49*, 8323-8336.

(10) Ghosh, A.K.; Fidanze, S.; Onishi, M.; Hussain, K.A. *Tetrahedron Lett.* **1997**, *38*, 7171-7174.

(11) Ghosh, A.K.; Onishi, M. *J. Am. Chem. Soc.* **1996**, *118*, 2527-2528.

(12) Targ, T. P.; Ellman, J. A. *J. Org. Chem.* **1999**, *64*, 12-13.

(13) X-ray crystal structures were determined by Allen D. Hunter and Rhea A. Nicklow at Youngstown State University.

(14) Still, W. C.; Kahn, M.; Mitra, A. *J. Org. Chem.* **1978**. *43*, 2923-2925.

A1

Figure 12a

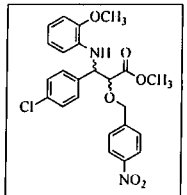

50a/51a

Figure 12b

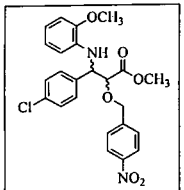

50a/51a

A2

Figure 13a

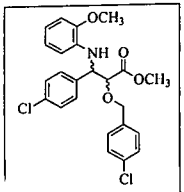

50b/51b

A3

Figure 13b

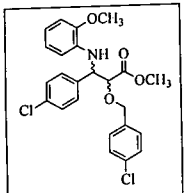

50b/51b

A4

Figure 14a

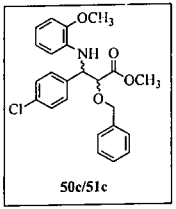

50c/51c

Figure 14b

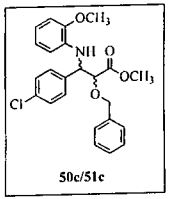

50c/51c

Figure 15a

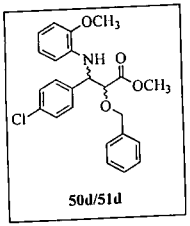

50d/51d

Figure 15b

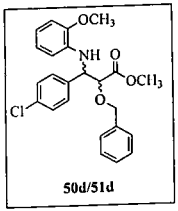

50d/51d

Figure 16a

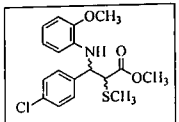

50f/51f

Figure 16b

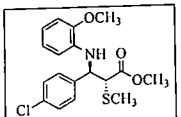

50f

Figure 16c

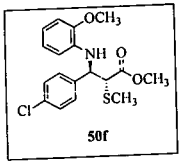

50f

Figure 17a

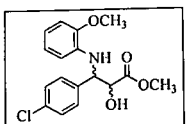

50g/51g

Figure 17b

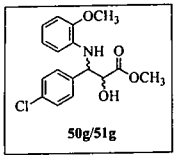

50g/51g

Figure 18a

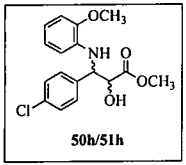

50h/51h

Figure 18b

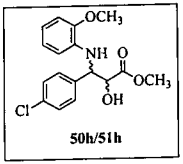

50h/51h

Figure 19a

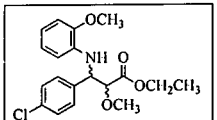

50i/51i

Figure 20a

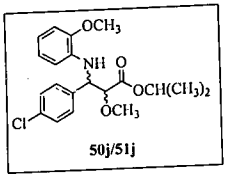

50j/51j

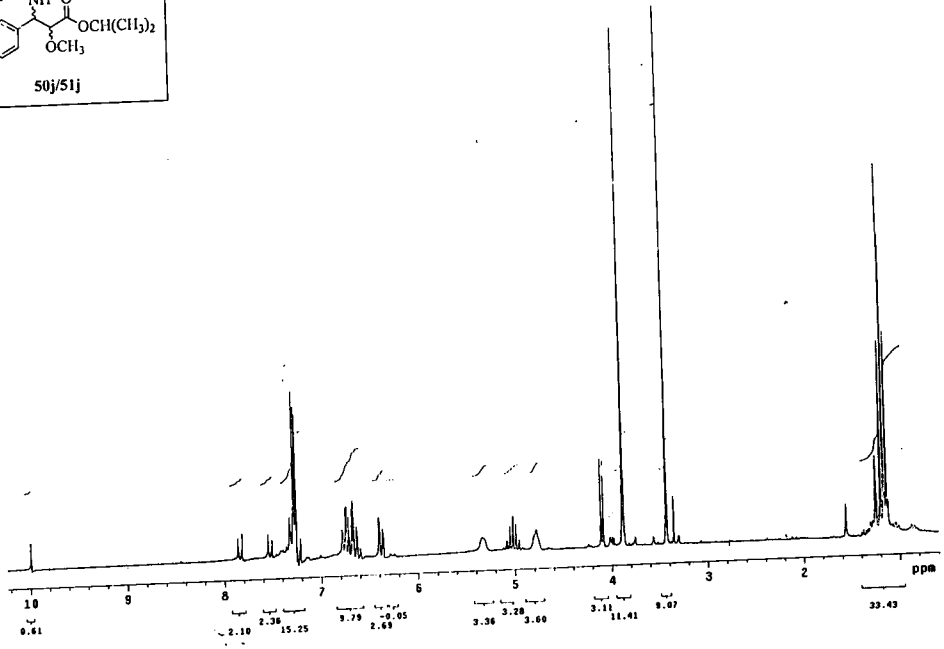

Figure 20b

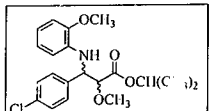

50j/51j

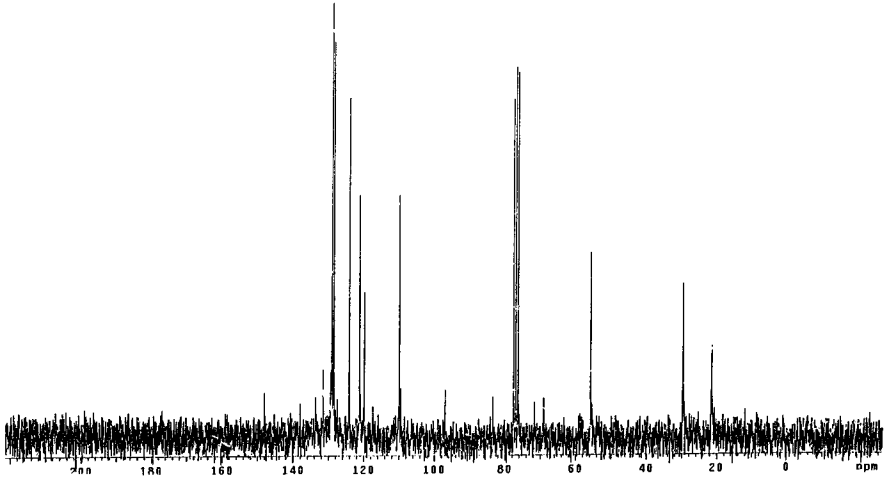

Figure 21a

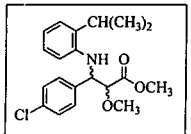

50k/51k

Figure 21b

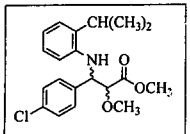

50k/51k

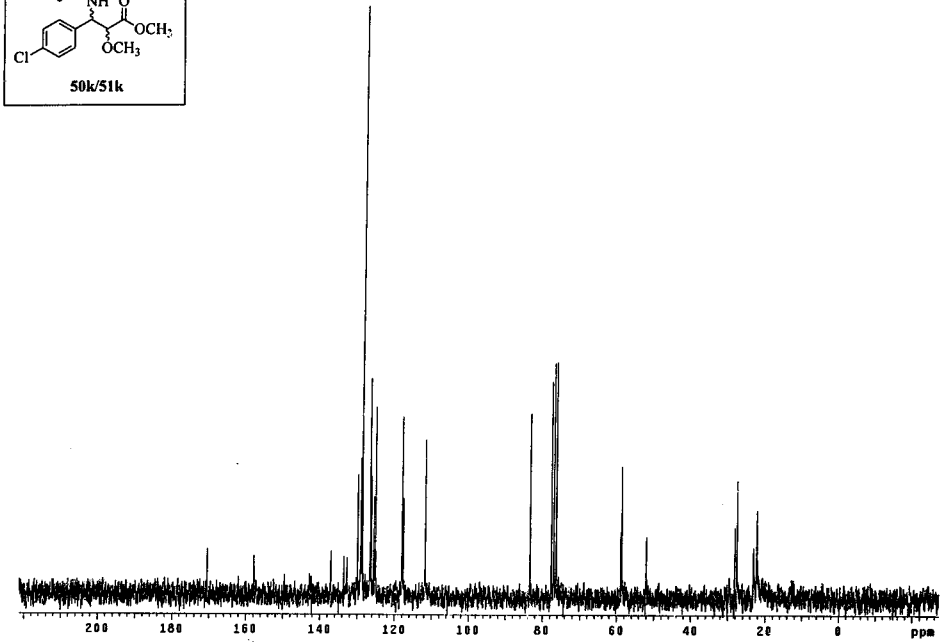

Figure 22a

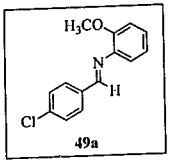

49a

Figure 22b

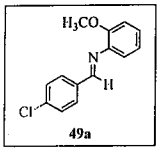

49a

Figure 23a

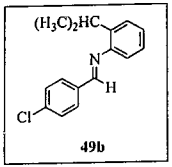

49b

Figure 23b

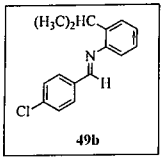

49b

Figure 24

Table xxx. Crystal data and structure refinement for 00adh01m.

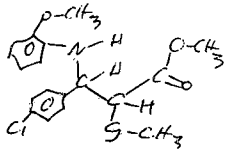

Identification code	00adh01m
Empirical formula	C18 H20 Cl N O3 S
Formula weight	365.86
Temperature	293(2) K
Wavelength	1.54178 A
Crystal system, space group	Orthorhombic, Pna2(1)
Unit cell dimensions	a = 11.0507(5) A alpha = 90 deg. b = 20.2424(7) A beta = 90 deg. c = 8.2956(3) A gamma = 90 deg.
Volume	1855.67(13) A^3
Z, Calculated density	4, 1.310 Mg/m^3
Absorption coefficient	3.002 mm^-1
F(000)	768
Crystal size	0.20 x 0.50 x 0.40 mm
Theta range for data collection	4.37 to 57.47 deg.
Limiting indices	-11<=h<=12, -22<=k<=22, -9<=l<=9
Reflections collected / unique	4223 / 2349 [R(int) = 0.0756]
Completeness to theta = 57.47	96.4 %
Absorption correction	Empirical
Max. and min. transmission	0.1503 and 0.0397
Refinement method	Full-matrix least-squares on F^2
Data / restraints / parameters	2349 / 1 / 266
Goodness-of-fit on F^2	1.876
Final R indices [I>2sigma(I)]	R1 = 0.1526, wR2 = 0.3624
R indices (all data)	R1 = 0.1536, wR2 = 0.3644
Absolute structure parameter	-0.07(6)
Extinction coefficient	0.004(2)
Largest diff. peak and hole	0.582 and -0.587 e.A^-3

Table 23. Atomic coordinates (x 10^4) and equivalent isotropic displacement parameters (A^2 x 10^3) for 00adh01m.
U(eq) is defined as one third of the trace of the orthogonalized Uij tensor.

	x	y	z	U(eq)
S	239(2)	4433(1)	3623(4)	82(1)
Cl	2745(4)	813(2)	-362(5)	125(2)
N	2796(8)	3678(5)	3729(13)	75(2)
C(1)	1385(8)	4041(5)	918(13)	66(2)
O(1)	1068(7)	3709(4)	-392(10)	81(2)
O(2)	2054(8)	4496(4)	926(11)	92(2)
C(2)	824(8)	3753(5)	2414(12)	63(2)
C(3)	1718(8)	3312(5)	3325(11)	61(2)
O(4)	4555(7)	4496(4)	4387(12)	90(2)
C(4)	1633(16)	3931(9)	-1892(17)	105(4)
C(5)	-935(11)	4018(7)	4661(19)	102(4)
C(6)	5463(14)	4976(9)	4720(30)	116(5)
C(11)	2001(7)	2690(4)	2384(10)	55(2)
C(12)	2969(9)	2636(6)	1339(12)	69(2)
C(13)	3198(11)	2073(7)	509(12)	80(3)
C(14)	2442(10)	1543(6)	679(12)	78(3)
C(15)	1435(10)	1574(5)	1674(16)	78(3)
C(16)	1236(9)	2152(5)	2525(12)	66(2)
C(21)	3631(7)	3478(5)	4846(10)	64(2)
C(22)	4585(8)	3906(6)	5203(14)	75(3)
C(23)	5494(12)	3737(9)	6275(17)	97(4)
C(24)	5436(14)	3121(10)	6994(16)	108(5)
C(25)	4519(15)	2689(10)	6664(14)	98(4)
C(26)	3592(10)	2865(6)	5576(12)	77(3)

Table 24. Bond lengths [A] and angles [deg] for 00adh01m.

S-C(5)	1.769(14)
S-C(2)	1.821(9)
Cl-C(14)	1.744(10)
N-C(21)	1.369(13)
N-C(3)	1.442(13)
N-H(1N)	0.74(15)
C(1)-O(2)	1.181(13)
C(1)-O(1)	1.325(13)
C(1)-C(2)	1.505(15)
O(1)-C(4)	1.463(17)
C(2)-C(3)	1.532(14)
C(2)-H(2)	0.80(13)
C(3)-C(11)	1.514(13)
C(3)-H(3)	0.90(13)
O(4)-C(22)	1.373(15)
O(4)-C(6)	1.424(16)
C(4)-H(4A)	1.3(3)
C(4)-H(4B)	1.1(2)
C(4)-H(4C)	1.1(2)
C(5)-H(5A)	0.9600
C(5)-H(5B)	0.9600
C(5)-H(5C)	0.9600
C(6)-H(6A)	0.8(3)
C(6)-H(6B)	1.0(2)
C(6)-H(6C)	1.2(3)
C(11)-C(12)	1.381(13)
C(11)-C(16)	1.384(14)
C(12)-C(13)	1.356(17)
C(12)-H(12)	0.94(14)
C(13)-C(14)	1.367(18)
C(13)-H(13)	0.96(15)
C(14)-C(15)	1.387(17)
C(15)-C(16)	1.384(16)
C(15)-H(15)	1.00(16)
C(16)-H(16)	1.04(13)
C(21)-C(26)	1.381(16)
C(21)-C(22)	1.396(15)
C(22)-C(23)	1.385(18)
C(23)-C(24)	1.38(3)
C(23)-H(23)	0.82(19)
C(24)-C(25)	1.37(3)
C(24)-H(24)	0.9300
C(25)-C(26)	1.411(18)
C(25)-H(25)	0.92(19)
C(26)-H(26)	0.86(15)
C(5)-S-C(2)	99.8(5)
C(21)-N-C(3)	124.2(9)
C(21)-N-H(1N)	121(10)
C(3)-N-H(1N)	108(10)
O(2)-C(1)-O(1)	124.4(10)
O(2)-C(1)-C(2)	123.7(10)
O(1)-C(1)-C(2)	111.8(8)

C(1)-O(1)-C(4)	115.4(9)
C(1)-C(2)-C(3)	111.5(7)
C(1)-C(2)-S	107.9(7)
C(3)-C(2)-S	113.4(7)
C(1)-C(2)-H(2)	110(8)
C(3)-C(2)-H(2)	102(9)
S-C(2)-H(2)	112(9)
N-C(3)-C(11)	112.1(8)
N-C(3)-C(2)	110.4(8)
C(11)-C(3)-C(2)	111.3(7)
N-C(3)-H(3)	116(7)
C(11)-C(3)-H(3)	99(7)
C(2)-C(3)-H(3)	108(8)
C(22)-O(4)-C(6)	118.7(11)
O(1)-C(4)-H(4A)	113(10)
O(1)-C(4)-H(4B)	113(10)
H(4A)-C(4)-H(4B)	131(10)
O(1)-C(4)-H(4C)	119(10)
H(4A)-C(4)-H(4C)	66(10)
H(4B)-C(4)-H(4C)	106(10)
S-C(5)-H(5A)	109.5
S-C(5)-H(5B)	109.5
H(5A)-C(5)-H(5B)	109.5
S-C(5)-H(5C)	109.5
H(5A)-C(5)-H(5C)	109.5
H(5B)-C(5)-H(5C)	109.5
O(4)-C(6)-H(6A)	111(10)
O(4)-C(6)-H(6B)	107(10)
H(6A)-C(6)-H(6B)	122(10)
O(4)-C(6)-H(6C)	97(10)
H(6A)-C(6)-H(6C)	118(10)
H(6B)-C(6)-H(6C)	99(10)
C(12)-C(11)-C(16)	117.7(9)
C(12)-C(11)-C(3)	123.3(9)
C(16)-C(11)-C(3)	119.0(8)
C(13)-C(12)-C(11)	122.0(11)
C(13)-C(12)-H(12)	120(8)
C(11)-C(12)-H(12)	118(8)
C(12)-C(13)-C(14)	119.6(10)
C(12)-C(13)-H(13)	132(8)
C(14)-C(13)-H(13)	108(8)
C(13)-C(14)-C(15)	121.1(10)
C(13)-C(14)-Cl	119.8(8)
C(15)-C(14)-Cl	119.1(10)
C(16)-C(15)-C(14)	118.0(11)
C(16)-C(15)-H(15)	123(8)
C(14)-C(15)-H(15)	119(8)
C(15)-C(16)-C(11)	121.7(10)
C(15)-C(16)-H(16)	124(6)
C(11)-C(16)-H(16)	114(6)
N-C(21)-C(26)	122.8(9)
N-C(21)-C(22)	118.0(10)
C(26)-C(21)-C(22)	119.2(9)
O(4)-C(22)-C(23)	123.3(11)
O(4)-C(22)-C(21)	114.7(9)
C(23)-C(22)-C(21)	122.0(13)
C(24)-C(23)-C(22)	117.8(14)

C(24)-C(23)-H(23)	127(10)
C(22)-C(23)-H(23)	115(10)
C(23)-C(24)-C(25)	121.6(12)
C(23)-C(24)-H(24)	119.2
C(25)-C(24)-H(24)	119.2
C(24)-C(25)-C(26)	120.3(16)
C(24)-C(25)-H(25)	127(10)
C(26)-C(25)-H(25)	113(10)
C(21)-C(26)-C(25)	119.0(14)
C(21)-C(26)-H(26)	122(10)
C(25)-C(26)-H(26)	119(10)

Symmetry transformations used to generate equivalent atoms:

Table 25. Anisotropic displacement parameters (A^2 x 10^3) for 00adh01m.
The anisotropic displacement factor exponent takes the form:
-2 pi^2 [h^2 a*^2 U11 + ... + 2 h k a* b* U12]

	U11	U22	U33	U23	U13	U12
S	67(2)	69(2)	109(2)	-19(1)	2(1)	5(1)
Cl	133(3)	112(3)	130(3)	-52(2)	-25(2)	50(2)
N	55(4)	70(4)	100(5)	1(4)	-22(4)	-9(4)
C(1)	47(5)	68(5)	82(6)	2(4)	-9(4)	-4(4)
O(1)	74(4)	96(5)	74(3)	-4(3)	1(4)	-8(4)
O(2)	87(5)	94(5)	96(5)	15(4)	-4(4)	-29(5)
C(2)	42(4)	62(5)	84(5)	-12(5)	-3(4)	-10(4)
C(3)	46(4)	66(5)	73(5)	-1(4)	6(4)	-4(4)
O(4)	66(4)	90(5)	114(6)	-15(4)	-25(4)	-15(4)
C(4)	101(9)	130(11)	84(8)	-5(7)	14(6)	-4(9)
C(5)	84(7)	115(9)	107(8)	-21(7)	18(7)	14(7)
C(6)	82(8)	120(11)	145(15)	-29(11)	-20(9)	-32(8)
C(11)	42(4)	59(5)	63(4)	4(3)	0(3)	2(4)
C(12)	53(5)	76(6)	77(5)	13(4)	1(4)	0(4)
C(13)	64(5)	109(8)	67(5)	0(5)	5(4)	30(6)
C(14)	78(7)	86(7)	71(5)	-10(5)	-7(5)	23(6)
C(15)	75(6)	63(5)	96(7)	-1(5)	-10(6)	0(5)
C(16)	61(5)	60(5)	76(5)	2(4)	1(4)	-3(4)
C(21)	49(4)	78(5)	64(5)	-12(4)	0(4)	12(4)
C(22)	57(5)	92(7)	76(5)	-23(6)	-8(4)	6(5)
C(23)	75(8)	124(11)	92(6)	-32(8)	-23(6)	10(7)
C(24)	97(9)	150(14)	77(6)	-15(8)	-29(6)	28(10)
C(25)	112(9)	119(10)	65(6)	3(6)	-1(6)	40(9)
C(26)	67(6)	96(7)	67(5)	-3(5)	3(4)	11(6)

Table 26. Hydrogen coordinates (x 10^4) and isotropic displacement parameters (A^2 x 10^3) for 00adh01m.

	x	y	z	U(eq)
H(1N)	2660(130)	4030(80)	3610(190)	90
H(2)	300(120)	3490(60)	2170(140)	75
H(3)	1320(110)	3130(60)	4160(150)	74
H(4A)	1000(200)	3830(110)	-3100(300)	157
H(4B)	2600(200)	3990(110)	-1800(300)	157
H(4C)	1300(200)	4390(110)	-2500(300)	157
H(5A)	-1338	4322	5368	153
H(5B)	-599	3662	5281	153
H(5C)	-1505	3845	3897	153
H(6A)	5300(200)	5340(140)	4300(400)	174
H(6B)	6300(200)	4750(120)	4500(400)	174
H(6C)	5400(200)	4940(140)	6200(400)	174
H(12)	3480(130)	3000(60)	1210(160)	82
H(13)	3890(130)	1930(70)	-110(170)	96
H(15)	950(130)	1160(80)	1860(180)	94
H(16)	470(110)	2240(60)	3210(150)	79
H(23)	5980(170)	4030(90)	6500(300)	116
H(24)	6036	2998	7721	130
H(25)	4470(160)	2260(90)	7000(200)	118
H(26)	3000(140)	2600(70)	5430(170)	92

Table 27. Torsion angles [deg] for 00adh01m.

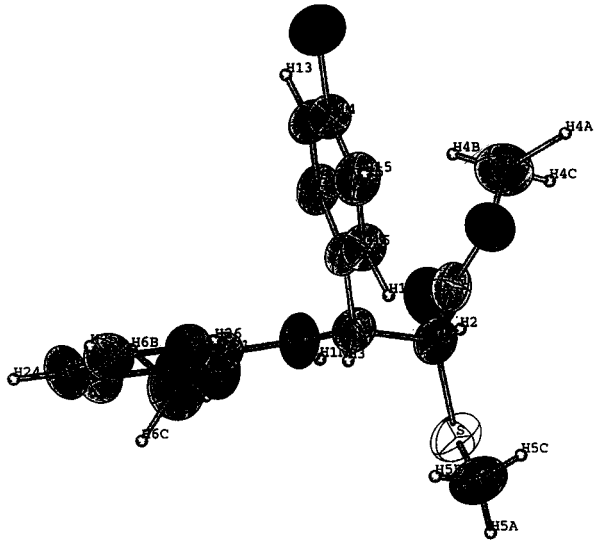
H13
H4A
H4B
H4C
H6B
H6C
H2
H5C
H5A

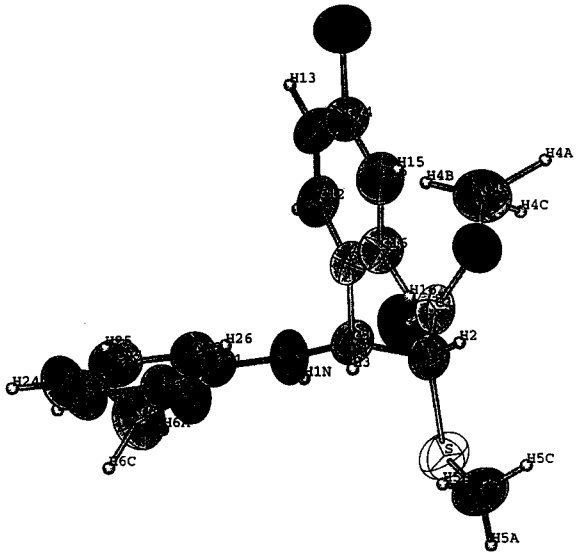
H13
H15
H4A
H4B
H4C
H26
H2
H1N
H5C
H5A
H6C

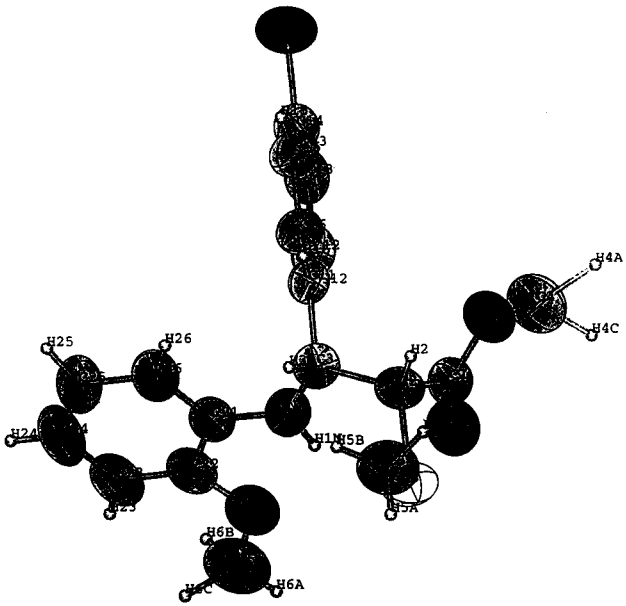
H4A
H4C
H25
H26
H2
H24
H6B
H6A

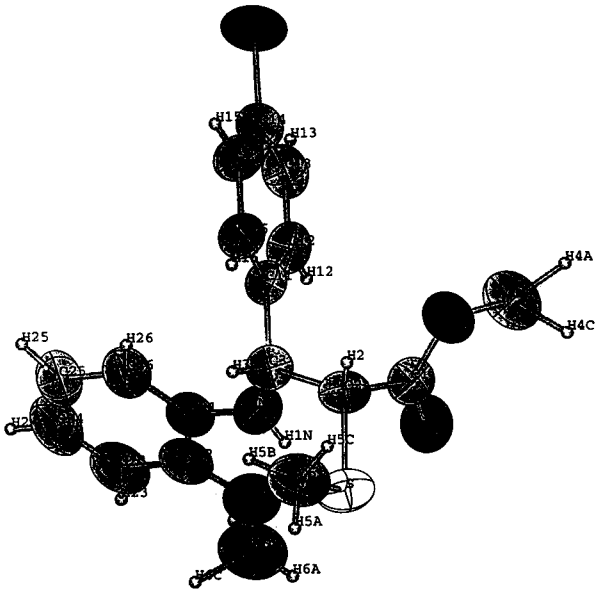
H13
H12
H4A
H4C
H25
H26
H2
H1N
H5C
H5B
H5A
H6A

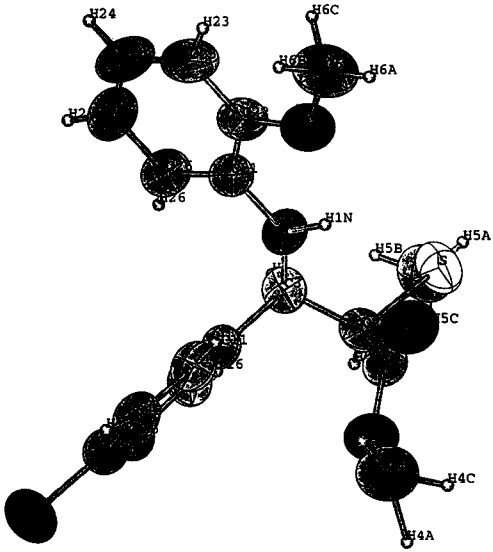
H24
H23
H6C
H6B
H6A
H1N
H5A
H5B
H5C
H4C
H4A

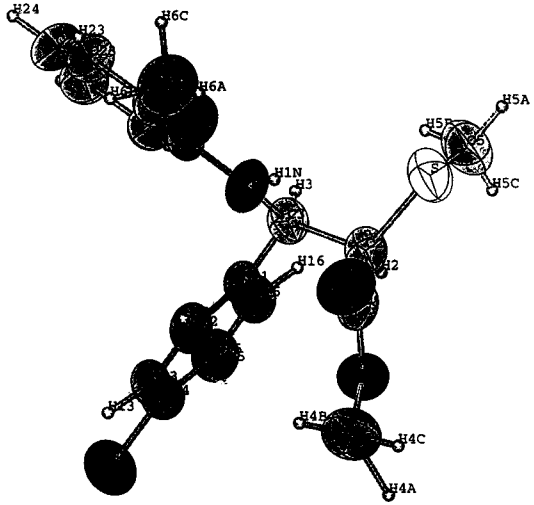
H24
H23
H6C
H6A
H5A
H5B
H5C
H1N
H3
H16
H2
H23
H4B
H4C
H4A